GLOBAL BIOGEOCHEMICAL CYCLES, VOL. 14, NO. 1, PAGES 477-498, MARCH 2000

Biological pump and vertical mixing in the Southern Ocean: Their impact on atmospheric CO_2

Ekaterina E. Popova

Southampton Oceanography Centre, Southampton, England

Vladimir A. Ryabchenko

St. Petersburg Branch, P.P. Shirshov Institute of Oceanology, Russian Academy of Sciences, St. Petersburg

Mike J.R.Fasham

Southampton Oceanography Centre, Southampton, England

Abstract. A global box model simulating nitrogen and carbon cycling in the ocean has been developed. The distinctive feature of the model is the detailed description of the seasonal cycles of the oceanic upper mixed layer (UML) ecosystem. Unlike other ocean regions, phytoplankton productivity in the Southern Ocean is assumed to be limited by low iron availability, leading to twofold decrease in the phytoplankton growth rate. Calculated ecosystem and carbon cycle characteristics are in a good agreement with available observational data and conceptual models of generalized phytoplankton seasonal cycles in the world ocean. The model estimates of the global ocean new production outside of shelf regions and the preindustrial atmospheric pCO_2 are 9.9 Gt C/yr and 282 ppm, respectively. Results of numerical experiments with the model showed that the potential new production which might be reached by allowing phytoplankton maximum growth rate to increase is 29 Gt C/yr (76% of this increase is contributed by the Southern Ocean) and corresponds to an atmospheric pCO_2 of 205 ppm; however, this would require an unrealistic tenfold increase in growth rate. The large contribution of the Southern Ocean is accounted for by the high-nutrient, low-chlorophyll (HNLC) conditions existing in this region caused by the high dissolved inorganic nitrogen concentrations below the UML, deep mixing during the austral summer, and iron limitation of phytoplankton productivity. A realistic (twofold) increase in the phytoplankton growth rate in the Southern Ocean which can be considered as a maximal effect of iron fertilization results in the lowering of atmospheric pCO_2 by only 10 ppm. Changes in the UML depth in the Southern Ocean (a wintertime shallowing and summertime deepening of the UML in comparison with preindustrial conditions) could lead to a decrease of atmospheric pCO_2 by 15 ppm at the most. The combined effect of iron fertilization and these changes in vertical mixing might constitute about 30-35 ppm, that is, less than one half of the lowering of 80 ppm during the last glaciation.

1. Introduction

There is considerable interest in the functioning of the carbon cycle at high latitudes in the ocean due to the great potential for changes of drawdown of atmospheric CO_2. Modern biological productivity in low-latitude areas is limited by the availability of nutrients; nutrient concentrations there are close to zero, and changes of their supply from below lead to equivalent changes in biological productivity, leaving surface concentrations of nutrients and the total inorganic carbon (TIC) almost unaffected [*Broecker*, 1982]. In contrast, biological productivity in the high-latitude areas is not limited by macronutrients, and changes of either physical factors (turbulent mixing, convection, advective transport) or biological factors (phytoplankton growth rate, zooplankton grazing, and others) could lead to significant changes of surface TIC concentrations and atmospheric pCO_2.

Paper number 1999GB900090.
0886-6236/00/1999GB900090$12.00

It is pertinent to note here that there is a substantial difference between the high latitudes of the Southern and Northern Hemispheres. The North Atlantic, with almost zero surface nutrient concentrations after a pronounced spring bloom and their renewal during the winter by deep mixing, is an example of regions which are called low-nutrient, high-chlorophyll (LNHC) areas. In contrast, the offshore Southern Ocean is a high-nutrient, low-chlorophyll (HNLC) region where a persistently low phytoplankton biomass occurs throughout the year and nutrients remain high and nonlimiting for phytoplankton growth. The Southern Ocean, with its low intensity of the biological pump in spite of the high surface nutrients, has been suggested as a major potential source for increasing the biological removal of carbon and, hence, a lowering of atmospheric pCO_2 [e.g., *Wenk and Siegenthaler*, 1985]. This idea about the key role of the high latitudes of the Southern Hemisphere in the potential changes of the ocean carbon cycle has been supported by a recent three-dimensional (3D) simulation of the response of the coupled ocean-atmosphere system to anthropogenic climate warming [*Sarmiento et al.*, 1998]. A large decrease of the ocean carbon sink was found in a vast region of the Southern Ocean.

At present it is unknown which of the two above mentioned factors (physical or biological) could play a crucial role in possible changes of surface TIC at high latitudes. According to *Toggweiler and Sarmiento* [1985] and *Francois et al.* [1997], these changes can be due to changes in vertical mixing and thus carbon supply into the surface ocean layer. *Peng and Broecker* [1991a,b] concluded that upwelling velocity and fate of the upwelled water are the major factors limiting uptake of atmospheric CO_2 by the ocean in response to iron fertilization of the Southern Ocean. Contrary to these dynamical hypotheses, *Martin et al.* [1990] considered changes in phytoplankton productivity due to variations in surface iron concentrations as a possible mechanism of changes in surface TIC concentrations. Iron is required for a number of biochemical processes in algae, such as nitrate reduction, electron transport, and chlorophyll synthesis [*Martin*, 1990; *Martin et al.*, 1990] and, although the amounts of iron required are small, there is growing evidence that the Southern Ocean may be iron-limited.

Model studies of the role of the Southern Ocean in the regulation of atmospheric CO_2 concentration have been carried out as applied both to natural variability processes of glacial to interglacial changes (see, for example, *Sarmiento and Toggweiler* [1984], *Siegenthaler and Wenk* [1984], *Knox and McElroy* [1984], *Toggweiler and Sarmiento* [1985], and *Keir* [1988]) and to the anthropogenic increase in atmospheric CO_2 resulting from fossil fuel combustion and terrestrial ecosystem disturbances [*Joos et al.*, 1991a,b; *Peng and Broecker*, 1991a,b; *Sarmiento and Orr*, 1991; *Sarmiento et al.*, 1998]. In all these studies, seasonal variations of the upper ocean ecosystem were not explicitly taken into account so that the effects of light supply and changes in the upper mixed layer UML depth mainly determining the seasonality of ocean biota could only be estimated approximately (estimates of this sort in the case of reduction of the rising atmospheric CO_2 concentrations by iron fertilization of the Southern Ocean have been obtained by *Peng and Broecker* [1991a,b] and *Joos et al.* [1991b]).

In this study we will try to refine the role of seasonal variations of marine biota in atmospheric pCO_2 regulation and to answer the following questions. What is the maximum potential new production of the modern world ocean and how much does the Southern Ocean contribute to it? How are these values affected by the seasonality of marine biota? Which factors are responsible for the formation of HNLC conditions in the Southern Ocean and could those that are determined by seasonal processes in the ocean lead to a significant change of atmospheric CO_2 concentrations?

The principal differences between our box model and previous models are the detailed description of the seasonal cycles of the UML ecosystem and the parameterization of the difference between ecosystem dynamics at high latitudes of the Southern and Northern Hemispheres. Another important feature of our model is an explicit description of alkalinity and total inorganic carbon changes associated with both components of the biological pump: production of organic carbon and biogenic formation of calcite in surface waters coupled with their decomposition in the deep layers. The proposed model is intermediate between few-box (as a rule, upper layer, deep ocean and high-latitude deep water formation region) models [e.g. *Siegenthaler and Wenk*, 1984; *Sarmiento and Toggweiler*, 1984; *Joos et al.*, 1991a,b] and multibox models which consider the Atlantic, Indian, and Pacific Oceans separately and subdivide each ocean into surface, intermediate, and deep water layers [*Bolin et al.*, 1983; *Broecker and Peng*, 1986; *Keir*, 1988].

2. Model Description

The structure of the model is based on that of a three-layer ventilated ocean model suggested by *Kagan and Maslova* [1991] for the investigation of the non-uniqueness of the ocean thermohaline circulation (OTHC). In the *Kagan and Maslova* [1991] model, the ocean is represented as a stack of three homogeneous outcropped boxes (deep, intermediate, and surface water masses) in each hemisphere. Volume and area of the outcrop region of each water mass are assumed to be fixed and equal, respectively, to 9% and 80% of the entire ocean volume and surface area for the

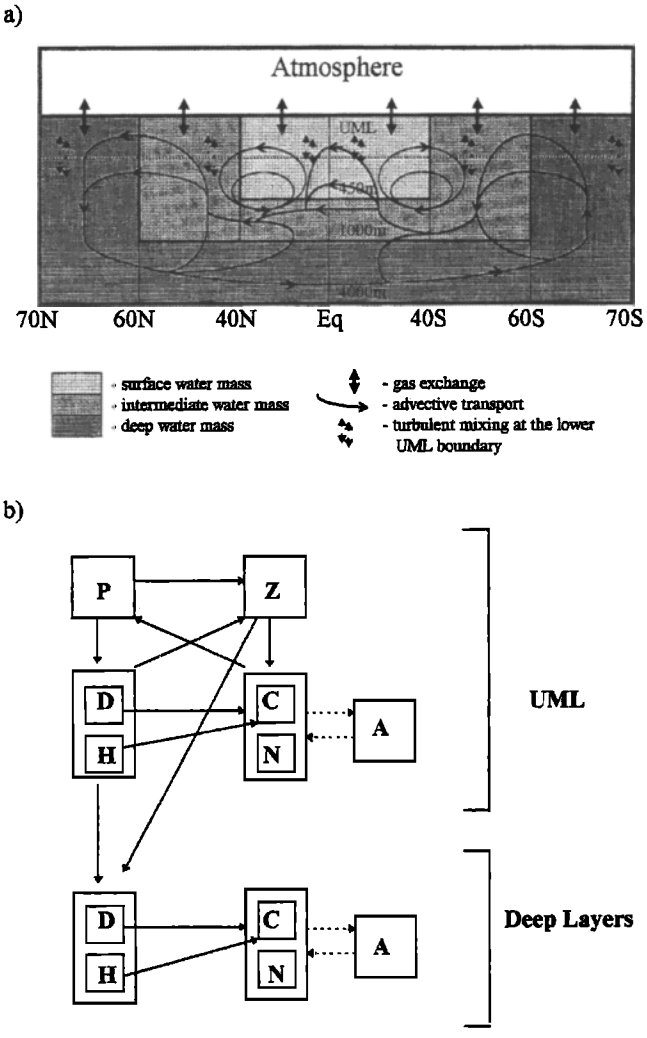

Figure 1. The ocean box model: (a) meridional cross section with boxes separated and physical processes considered; (b) ecosystem submodel.

surface water mass, 16% and 16% for the intermediate water mass, and 75% and 4% for the deep water mass [*Levitus*, 1982]. For our purposes this structure was modified as follows: (1) an UML was placed at the top of the outcrop region of each water mass, and (2) intermediate and deep water masses were divided into two boxes each (Figure 1a). The latter modification allows one to take into account the meridional gradients of biogeochemical characteristics in the intermediate and deep water masses. These gradients are formed due to the gravitational sinking of detritus, which happens much faster than the mixing of water masses due to isopycnical diffusion. In order to prescribe external forcing functions and to compare model results with observational data, boundaries between outcropped boxes at the ocean surface have to be determined. Hereafter we conventionally assume that the latitudinal extension of the outcrop areas are 0^o-40^o, 40^o-60^o and 60^o-70^o, respectively, for surface, intermediate, and deep water masses in each hemisphere (see Figure 1a).

The model prognostic variables include phytoplankton P, zooplankton Z, the organic part of detritus (soft tissue) D, dissolved inorganic nitrogen (DIN) N, oceanic TIC C, the inorganic part of detritus (calcareous hard parts) H, total alkalinity A, and atmospheric carbon dioxide C_a. The model describes the oceanic cycles of nitrogen and carbon including the biological pump (the formation of particulate organic matter and $CaCO_3$ in the upper ocean, their export to depth, and degradation of particulate organic matter and dissolution of $CaCO_3$ in the deep ocean), oceanic transport processes (advection by the thermohaline circulation and vertical mixing in the upper ocean), and exchange of CO_2 between the ocean and atmosphere. A temperature effect on the phytoplankton growth rate as well as on the solubility of CO_2 and $CaCO_3$ and the dissolution of the carbon and borate acids is taken into account. The division of the detritus into two forms (soft and hard tissue) was needed because of the difference in their regeneration depths. It should be emphasized that D and H are different parts of one particle.

The principal processes considered by the model are (Figure 1): gas exchange between ocean and atmosphere, advective transport, entrainment and detrainment at the lower boundary of the UML, primary production of phytoplankton, phytoplankton and zooplankton mortality, grazing of zooplankton, detritus remineralization, gravitational sinking of particles, degradation of the detritus hard parts, and inorganic carbon chemistry processes. The equations describing the budget of the state variables in each box are given in the appendix.

2.1. Parameterizations of the Physical Processes

The scheme of the advective transport represents an idealized zonally averaged thermohaline circulation in the Atlantic Ocean. The circulation (Figure 1a) is characterized by two cells in the Northern Hemisphere providing downwelling in the high latitudes and upwelling in the low latitudes and midlatitudes and two cells in the Southern Hemisphere ensuring upwelling in the high and low latitudes and downwelling in the midlatitudes. Cross-equatorial transport is characterized by the flow of deep water from the Northern to the Southern Hemisphere and reverse flux of the intermediate and surface waters, including the UML [*Weaver and Hughes*, 1992; *Kagan and Maslova*, 1991]. Volume transport values between neighboring water masses excepting the cross-equatorial volume transport were taken from the model of *Kagan and Maslova* [1991]. The cross-equatorial volume transport in the deep water is treated as an adjustable parameter in order to provide the observed difference in DIN and carbon concentrations between

the Northern and Southern Hemispheres. The circulation scheme accepted here might be considered as a simplified oceanic conveyor belt [cf. *Broecker and Peng*, 1982]. Our model reflects the scheme of the conveyor, except that it involves the Atlantic Ocean only, cutting off the Indian and Pacific Oceans (Figure 1).

Turbulent fluxes at the lower boundary of the UML due to entrainment and detrainment are parameterized in terms of the entrainment velocity [see *Ryabchenko et al.*, 1998].

2.2. Parameterizations of the Biogeochemical Process

The carbon flux at the ocean-atmosphere boundary is assumed to be proportional to the difference between the partial pressure of CO_2 in the atmosphere and that in the UML, the gas transfer coefficient being taken to be dependent on the wind friction velocity. In order to calculate the partial pressure of CO_2 in the UML from total alkalinity and total inorganic carbon, traditional carbon and borate seawater chemistry relationships are used [*Broecker and Peng*, 1982].

The basis for most if not all of modern hydrodynamic-biogeochemical models is an assumption that the differences in the annual cycle of phytoplankton productivity between different ocean regions are determined by changes in physical forcing [see *Sarmiento et al.*, 1993; *Six and Maier-Reimer*, 1996; *Ryabchenko et al.*, 1998; *Palmer and Totterdell*, 1999]. The ecosystem behavior then is described using some globally uniform parameterizations of the biological sources and sinks with one and the same set of model parameter values. However, this appears not to be the case for the Subantarctic water ring (which constitutes about a tenth of the global ocean area) and the open Subarctic Pacific, where the phytoplankton regime differs from much of the North Atlantic at the same range of latitudes. In fact, low surface chlorophyll concentrations and the high level of nutrients throughout the year are typical for offshore in the Subantarctic region [*Banse*, 1996] and in the open Subarctic Pacific, as observed at Ocean Weather Station (OWS) P [*Parsons and Lalli*, 1988; *Frost*, 1993], whereas in the midlatitude and high-latitude North Atlantic region there is a pronounced spring bloom and summer DIN concentrations are low enough to limit primary production, as observed at OWS I [*Parsons and Lalli*, 1988; *Williams*, 1988] and the Joint Global Ocean Flux Study (JGOFS) North Atlantic Bloom Experiment station at 47°N, 20°W [*Lochte et al.*, 1993]. Taking into consideration that our model does not discriminate between the Atlantic and Pacific Oceans and is appropriate to the Atlantic to a greater extent than the Pacific, hereafter we shall concentrate on the difference between the Subarctic Atlantic and Subantarctic regions. Seasonal changes in the UML depth and solar irradiance at the sea surface are rather similar in either region considered (for the UML depth this is seen from comparison of Figures 5 and 7). The main difference in the physical forcing is the much shallower summer value and the deeper winter value of the UML depth at the high latitudes and midlatitudes of the North Atlantic relative to the Subantarctic region. As will be shown later, our model with globally uniform parameters of the ecosystem cannot simulate the observed different seasonal cycles of primary production and nutrients between the above regions. As was suggested by *Martin* [1990], the present high level of nutrients in the Southern Ocean may result from scarcity of iron (Fe) due to the comparatively low atmospheric transport of Fe-containing dust to this region. As summarized by *Banse* [1991, 1996], the specific phytoplankton growth rate in the Subantarctic region may be depressed by low iron availability, but addition of the element does not more than double it. In order to account for this feature of phytoplankton productivity in the open Subantarctic region, the initial slope α of the $P - I$ curve and maximum phytoplankton growth rate V_p for the surface outcrop boxes of deep and intermediate water masses of the Southern Hemisphere (their area is exactly 10% of the model ocean surface area) are reduced by one half relative to their standard values, all parameterizations of biological processes as well as values of other model parameters being the same everywhere. The decrease of α and V_p reduces the specific phytoplankton growth rate by about one half (see equations (A22)-(A24) in the appendix). Parameterizations of the inner sources and sinks of the phytoplankton, zooplankton, detritus soft tissue, and DIN in the UML are taken from *Fasham et al.* [1993] and *Fasham* [1995] and are given in the appendix.

Inner sources and sinks of the DIN and organic part of the detritus in the intermediate and deep boxes are determined by the remineralization of the organic part of the detritus. Inner sources and sinks of the dissolved inorganic carbon in all boxes are assumed to be determined by the same processes as for DIN according to the Redfield ratio. In addition, inorganic carbon is considered to be changed as a result of the uptake of dissolved $CaCO_3$ by phytoplankton in the UML and degradation of the inorganic part of the detritus, which is controlled by the degree of undersaturation of seawater with respect to calcite [*Heinze et al.*, 1991]. The inner sources and sinks of the inorganic part of the detritus in the UML are determined by the nonassimilated fraction of zooplankton grazing, phytoplankton natural mortality, the part of zooplankton losses remaining in the UML, and the dissolution of $CaCO_3$. In the boxes below the UML, inner sources and sinks of H are associated with dissolution only. Alkalinity changes are assumed to be due to changes

of DIN concentration, dissolution of the inorganic part of the detritus, and uptake of the bicarbonate ions for primary production.

The particle flux at the lower boundary of the UML consists of the fast sinking part of the zooplankton losses and gravitational sinking of the detritus soft and hard tissue with the detritus sinking velocity of 4 m/d. There is no precipitation of detritus on the ocean bottom.

2.3. External forcing

The model requires that the forcing functions (the annual cycles of solar radiation, the UML depth, wind friction velocity, sea surface temperature, and salinity) be specified. The annual cycles of solar radiation averaged over the outcrop areas were calculated as a function of area-averaged latitude, cloudiness, and air temperature using the technique of *Girdjuk et al.* [1992]. The air temperature was assumed to be fixed and equal to 5^o, 15^o and 20^oC, respectively, for the outcrop areas of the deep, intermediate, and surface water masses. The cloudiness was constant and equal to 6 oktas. The annual cycles of the wind friction velocity were taken from *Han and Lee* [1981].

The UML depth was defined as the depth at which the density σ_t is 0.25 less than the sea surface density. Mean monthly UML depth values in the outcrop areas were estimated from mean monthly temperature and salinity distributions at standard horizons taken, respectively, from *Levitus and Boyer* [1994] and *Levitus et al.* [1994] and averaged over the outcrop area considered. To simplify calculations, the temporal changes in the UML depth were reconstructed through an approximation of its monthly means obtained by a simple function of time dependent on two parameters, maximum and minimum values of the UML depth during the annual cycle (see (A39) in the appendix). Values of sea surface temperature and salinity at any moment of the annual cycle are calculated by linear interpolation between monthly means obtained as described above.

3. Control Run

The control run was performed in two stages. At first, an equilibrium state of the ocean relevant to the preindustrial period, when the globally averaged value of atmospheric pCO_2 was about 280 ppm (with fluctuations up to 10 ppm [*Houghton et al.* 1995]), was obtained by the integration of the model equations for 70,000 years. The calculated equilibrium atmospheric pCO_2 of 282 ppm turned out to be close to the estimated value. The results of this run were used as initial conditions for all subsequent numerical experiments. In order to compare model results with observations dated from the industrial period, the integration of the model equations for oceanic variables has been continued under the prescribed mean annual values of atmospheric pCO_2 observed in this period [*Houghton et al.*, 1995].

3.1. Mean Annual Characteristics

Calculated mean annual values of ecosystem and carbon cycle characteristics are given in Figures 2-4 and Table 1 together with Geochemical Ocean Section Study (GEOSECS) data obtained in 1973 for nitrate (which constitutes the majority of DIN), total inorganic carbon and alkalinity [*Bainbridge*, 1981; *Broecker et al.*, 1982], climatological mean annual data for nitrate from the Levitus archive [*Conkright et al.*, 1994], and the ocean surface pCO_2 distribution observed in 1990 [*Takahashi et al.*, 1997]. The initial GEOSECS and Levitus archive data were averaged over the model boxes for both the Atlantic Ocean only and the world ocean as a whole. The GEOSECS data for the UML were not used in the processing because they do not cover all seasons and averaging them could give distorted estimates of concentrations considered.

3.1.1. Modeled distribution of DIN. The modeled distribution of DIN (Figure 2) has the following gross features that can be seen in the GEOSECS and Levitus data for the Atlantic Ocean: (1) the pronounced maximum in the intermediate water mass of the Northern Hemisphere (0^o-40^oN), (2) the pronounced horizontal gradient within the deep water mass in the Northern Hemisphere and nearly homogeneous distribution in the Southern Hemisphere, and (3) the strong cross-equatorial gradient of DIN in the deep and intermediate water mass, reflecting the significant difference in nutrient content between the Southern and Northern Hemispheres. This difference is a consequence of the simultaneous operation of the biological pump and the thermohaline-driven conveyor belt [*Broecker and Peng*, 1982] initiated by the formation of deep waters in the high latitudes of the North Atlantic. The deep waters flow from the North Atlantic to high latitudes of the Southern Hemisphere and further to the North Pacific. A compensation flow of the opposite direction occurs in the upper 1000 m. The DIN concentration in the deep ocean increases along the pathway toward the North Pacific due to remineralization of sinking organic matter [*Broecker and Peng*, 1982].

As already noted, in our model the pattern is also working if one imagines that the conveyor involves the Atlantic Ocean only, cutting off the Indian and Pacific Oceans. A steady state is achieved when output advective transport of deep DIN concentrations from the North Atlantic is in a balance with input advective transport in the upper 1000 m. Since, for the steady state of the system, the deep water volume transport from the Northern to Southern Hemisphere is equal to

a) Control Run

	60-70N	40-60N	0-40N	0-40S	40-60S	60-70S
UML	10.8	7.9	0.15	0.18	23.6	29.1
z_{UML}-450m	16.0	16.4	6.5	8.6	25.5	30.2
450-1000m	16.0	16.4	27.5	30.0	25.4	30.2
1000-4000m	16.0	21.6		30.2		30.2

b) World Ocean Atlas 1994 data (World ocean)

	60-70N	40-60N	0-40N	0-40S	40-60S	60-70S
UML	6.3	6.5	1.3	1.5	15.6	23.8
z_{UML}-450m	14.8	27.0	15.7	12.2	26.3	31.9
450-1000m	14.8	27.0	33.0	28.7	26.3	31.9
1000-4000m	14.8	32.9		31.9		31.9

c) World Ocean Atlas 1994 data (Atlantic)

	60-70N	40-60N	0-40N	0-40S	40-60S	60-70S
UML	5.8	3.3	1.7	2.3	16.6	23.9
z_{UML}-450m	12.5	14.5	15.2	15.8	28.2	32.5
450-1000m	12.5	14.5	28.3	32.0	28.2	32.5
1000-4000m	12.5	19.7		31.1		32.5

d) GEOSECS (World Ocean)

	60-70N	40-60N	0-40N	0-40S	40-60S	60-70S
z_{UML}-450m	14.9	22.4	12.9	10.5	26.5	31.8
450-1000m	14.9	22.4	31.7	30.4	26.5	31.8
1000-4000m	14.9	30.5		32.3		31.8

e) GEOSECS (Atlantic)

	60-70N	40-60N	0-40N	0-40S	40-60S	60-70S
z_{UML}-450m	14.9	15.4	7.8	11.2	28.7	32.1
450-1000m	14.9	15.4	23.7	30.4	28.7	32.1
1000-4000m	14.9	19.7		28.4		32.1

Figure 2. The dissolved inorganic nitrogen (DIN) concentration (mmol/m^3) in the model boxes: (a) control run, (b) data from *Conkright et al.*, [1994] for the world ocean, (c) data from *Conkright et al.*, [1994] for the Atlantic Ocean, (d) GEOSECS data for the world ocean, and (e) GEOSECS data for the Atlantic Ocean.

the opposite volume transport in the upper 1000 m, such a balance is possible if deep DIN concentration in the Northern Hemisphere is equal to the averaged upper 1000 m concentrations in the Southern Hemisphere. Taking into account the fact that DIN concentrations increase with depth, nitrogen content should be significantly higher in the Southern than in the Northern Hemisphere. The results obtained confirm this conclusion.

The main discrepancy between the calculated and observed DIN concentrations occurs in the surface water mass below the UML between the equator and 40°N and 40°S. The most likely explanation for the underestimation of the DIN concentration in this area is the absence of any parameterization of the effect of wind-driven upwelling. Similar underestimated concentrations are seen in the spatial distribution of the total inorganic carbon (Figure 3).

3.1.2. Primary and new production, f ratio and particle flux. *Sundquist* [1985] listed a collection of early global ocean annual primary production estimates based on ^{14}C incubation data from cruises, which are well spread between 20 and 45 Gt C/yr with one estimate of 60-80 Gt C/yr. A later estimate of global primary production of about 27 Gt C/yr was derived from about 8000 ^{14}C data by *Berger et al.* [1987]. Two recent global primary production estimates based on sea surface chlorophyll concentrations derived from Coastal Zone Color Scanner (CZCS) data are 45 to 50 Gt C/yr [*Longhurst et al.*, 1995] and 37 to 46 Gt C/yr [*Antoine et al.*, 1996]. The modeled global primary production is equal to 31.1 Gt C/yr (Table 1). This value is in the middle of estimates summarized by *Sundquist* [1985], somewhat higher than the estimate of *Berger et al.* [1987], and 1.2-1.6 times less than the two satellite-based estimates. However, according to *Longhurst et al.* [1995], 14.4 Gt C/yr is related to the coastal and polar Arctic domains which are not allowed for by our model, as well as a part of the polar region that is ice covered in winter with a rate of primary production of about 2-3 Gt C/yr. If this production is removed from the total of 45-50 Gt C/yr, the model estimate matches the observed value of 27-33 Gt C/yr for the open ocean.

The salient feature of the latitudinal pattern of calculated primary production (Table 1) is that the values per square meter at midlatitudes and high latitudes of the Northern Hemisphere are 2-3 times higher than at the same latitudes of the Southern Hemisphere. As we have already discussed in the preceding section, the reason for the difference is higher UML depths during the summer and reduced values of the α and V_p parameters in the Southern Ocean because of the assumed low concentrations of dissolved iron there which limit the phytoplankton growth rate.

The modeled value of global annual new production of 9.9 Gt C/yr agrees well with estimates derived from global 3-D hydrothermodynamics-biogeochemical models, which are from 12 to 15 Gt C/yr [*Najjar et al.*, 1992], 11.1 Gt C/yr [*Six and Maier-Reimer*, 1996], and 9.4 Gt C/yr [*Palmer and Totterdell*, 1999].

The model outcrop boxes reflect all three contrasting types of regions with respect to new production [*Ducklow*, 1995]: (1) regions where surface nutrients are renewed each winter due to the deep mixing and depleted in the spring by biological utilization (high latitudeand midlatitude boxes of the Northern Hemisphere); (2) HNLC regions where phytoplankton stays low throughout the year in spite of high surface nutrients (high latitude and mid-latitude boxes of the Southern Hemisphere), and (3) large oligotrophic regions with a permanently nutrient-depleted euphotic zone (low latitude boxes in both hemispheres). How-

Table 1. Mean Annual Characteristics of the Carbon Cycle

	Model Area							
	Northern hemisphere			Southern hemisphere			Global	Atmo-
	High Latitude	Mid-latitude	Low Latitude	Low Latitude	Mid-latitude	High Latitude	Value	sphere
pCO_2 in the UML (model preindustrial values), ppm	263	276	285	282	284	263		282
pCO_2 in the UML (model, 1990), ppm	311	343	353	352	340	292		352
pCO_2 in the UML (data, 1990 [Takahashi et al., 1997]), ppm	311	333	360	362	345	342		352
Primary production, GtC/yr	1.1	5.7	11.0	11.8	1.4	0.2	31.1	
Primary production, $gC/m^2/d$	0.49	0.63	0.24	0.24	0.26	0.15	0.28	
New production, GtC/yr	0.5	2.0	3.3	3.5	0.5	0.1	9.9	
f ratio	0.42	0.36	0.30	0.30	0.35	0.46	0.31	

ever, the areas of the outcrop boxes do not accurately approximate the relative areas of the mentioned types. According to the classifications of primary domains of the global pelagic ecosystem suggested by *Longhurst et al.* [1995], areas where production is controlled by the high stability of a shallow pycnocline and phytoplankton bloom is not lightlimited cover about half of the total ocean. *Francois et al.* [1997] referred to nutrient-depleted subtropical regions as being 60% of the total area. In our model such regions constitute 80% of the ocean surface and thus leave only 10% to the regions with the intensive spring bloom and nutrients supplied by the deep winter mixing and 10% to the HNLC regions (which are suggested to be about 18% of the total ocean area by *Martin* [1990] and 10% by *Banse* [1996]). According to the three independent field estimates obtained by *Francois et al.*[1997], the new production in the vast, nutrient-depleted subtropical ocean (covering about 60% of the total ocean area) is 5-6 Gt C/yr (about 2 mol C m^{-2} yr^{-1}), accounting for up to half of the global value. Our model agrees reasonably with these observed values and predicts 6.8 Gt C/yr (2.2 mol C m^{-2} yr^{-1}) in the low-latitude surface boxes (see Table 1).

The modeled values of the mean annual f ratio in the UML boxes increase from low to high latitudes (Table 1), but do not show a correlation with the latitudinal distribution of primary production, thus not supporting the idea that areas where primary production is high should have a higher f ratio [*Eppley and Peterson*, 1979]. The global calculated f ratio of 0.31 falls in the range between its lower values in 3-D global models (0.25 and 0.15 as obtained, respectively, by *Six and Maier-Reimer* [1996] and *Palmer and Totterdell* [1999]) and its higher values in some 3-D basin models (0.43 and 0.45 as obtained, respectively, by *Sarmiento et al.* [1993] for the North Atlantic and by *Ryabchenko et al.* [1998] for the Arabian Sea). These differences are probably due to different model parameters that change the amount of recycling of the organic matter in the UML.

The particulate (detritus soft tissue) sinking flux can be calculated in our model at the lower boundary of the surface water mass, z =450 m, or at the lower boundary of the intermediate water mass, z =1000 m, but not anywhere in the deep water mass, which is lacking in horizontal boundaries (see Figure 1a). However, *Lampitt and Antia* [1996], using the *Martin et al.* [1987] dependence of the particulate sinking flux on vertical coordinate, recalculated the available sediment trap data for z=2000 m. According to their estimate, the flux outside of the polar domain ranges from 0.38 to 4.2 $g/m^2/yr$. The modeled value of the flux at z=1000 m averaged over the midlatitude and low-latitude boxes of both hemispheres is equal to 1.1 g m^{-2} yr^{-1} (and to about 0.6 g m^{-2} yr^{-1} for z=2000 m, being recalculated using the Martin dependence), thus falling within the above range.

3.1.3. Carbon cycle characteristics. The model estimate for the oceanic uptake of CO_2 corresponding to 1990 is 2.1 Gt C/yr, in good agreement with the other model-based estimates (2.0±0.6 Gt C/yr, [*Siegenthaler and Sarmiento*, 1993]). The latitudinal distributions of the observed [*Takahashi et al.*, 1997] and modeled ocean surface pCO_2 corresponding to 1990 are given in Table 1. As seen, the model reproduces the latitudinal distribution of oceanic pCO_2 with reasonable accuracy.

a) Control Run (pre-industrial)

atmosphere	282 ppm					
	60-70N	40-60N	0-40N	0-40S	40-60S	60-70S
UML	2076	2044	1878	1928	2140	2198
z_{UML}-450m	2107	2102	1933	1944	2154	2200
450-1000m	2107	2102	2195	2185	2154	2200
1000-4000m	2107	2174		2195		2200

b) Control Run (1973)

atmosphere	335 ppm					
	60-70N	40-60N	0-40N	0-40S	40-60S	60-70S
UML	2099	2076	1915	1968	2169	2235
z_{UML}-450m	2127	2129	1965	2026	2177	2219
450-1000m	2127	2129	2200	2198	2177	2219
1000-4000m	2127	2175		2197		2219

c) GEOSECS (World Ocean)

	60-70N	40-60N	0-40N	0-40S	40-60S	60-70S
z_{UML}-450m	-	2209	2123	2097	2186	2256
450-1000m	-	2209	2253	2220	2186	2256
1000-4000m	-	2296		2279		2256

d) GEOSECS (Atlantic)

	60-70N	40-60N	0-40N	0-40S	40-60S	60-70S
z_{UML}-450m	-	2168	2116	2100	2186	2249
450-1000m	-	2167	2195	2220	2186	2249
1000-4000m	-	2196		2224		2249

Figure 3. Total inorganic carbon (TIC) concentration (mmol/m^3) in the model boxes (a) calculated in the control run for preindustrial state, (b) calculated in the control run for 1973, (c) observed from GEOSECS data for the world ocean, and (d) observed from GEOSECS data for the Atlantic Ocean.

The main discrepancy occurs at the high latitudes of the Southern Hemisphere where the model underestimates oceanic pCO_2, probably due to the underestimated values of the carbon to alkalinity ratio. The paucity of the data for this area does not allow us to specify which of these two model characteristics provides the main contribution to this discrepancy.

The simulated spatial distribution of TIC shows all the gross features inherent in the GEOSECS data for the Atlantic (Figure 3): TIC concentrations increase with latitude in the upper ocean (surface to 450 m), decrease from the equator to midlatitudes in the intermediate layer (450-1000 m), and increase from the north to south in the deep ocean (1000-4000 m). The two first features are also seen in the GEOSECS data for the world ocean, but in this case, because of the large contribution of the Pacific, latitudinal changes of TIC in the deep ocean are opposite.

The observed distribution of total alkalinity (Figure 4) does not demonstrate any clear latitudinal trends, and significant increase of alkalinity with depth (by 55-95 mmol/m^3 between surface and deep water boxes) only occurs in the Atlantic. The model simulates this depth dependence with fair accuracy everywhere except the midlatitudes of the Southern Hemisphere. The reason for the discrepancy is unknown, but the GEOSECS alkalinity data might not be well representative because of a paucity of observations.

3.2. Seasonal Evolution

The simulated annual cycles of primary production, phytoplankton, and DIN, together with the prescribed UML depth in the surface model boxes, are shown in Figures 5-7. As a basis for qualitative comparison between the simulated phytoplankton annual cycle and the data, we used the conceptual models of generalized phytoplankton seasonal cycles in the world ocean obtained by *Longhurst* [1995] from the climatological CZCS chlorophyll data. In the Longhurst analysis, eight distinct groups were typified. Specific features of each group are principally dictated by the seasonal cycles of physical processes such as vertical mixing within the upper kilometer and solar radiation. Five of these groups fall within the shelf and polar domains which are not included in our model, and only three others belonging to low latitudes and midlatitudes of the open ocean will be considered here.

The seasonal cycles of primary production, phytoplankton biomass and DIN in the model high-latitude and midlatitude boxes of the Northern Hemisphere (Figure 5) coincide very closely and share the principal features of Longhurst model 2 (midlatitude nutrient-

a) Control Run

UML	2311	2300	2300	2363	2403	2416
z_{UML}-450m	2308	2313	2297	2358	2403	2415
450-1000m	2308	2313	2333	2398	2403	2415
1000-4000m	2308	2361		2414		2415

b) GEOSECS (World Ocean)

	60-70N	40-60N	0-40N	0-40S	40-60S	60-70S
z_{UML}-450m	-	2333	2393	2351	2323	2356
450-1000m	-	2333	2343	2308	2323	2356
1000-4000m	-	2346		2352		2356

c) GEOSECS (Atlantic)

	60-70N	40-60N	0-40N	0-40S	40-60S	60-70S
z_{UML}-450m	-	2319	2340	2335	2318	2411
450-1000m	-	2319	2319	2319	2318	2411
1000-4000m	-	2394		2412		2411

Figure 4. The total alkalinity (mmol/m^3) in the model boxes (a) calculated in the control run, (b) observed (GEOSECS data) for the world ocean, and (c) observed (GEOSECS data) for the Atlantic Ocean.

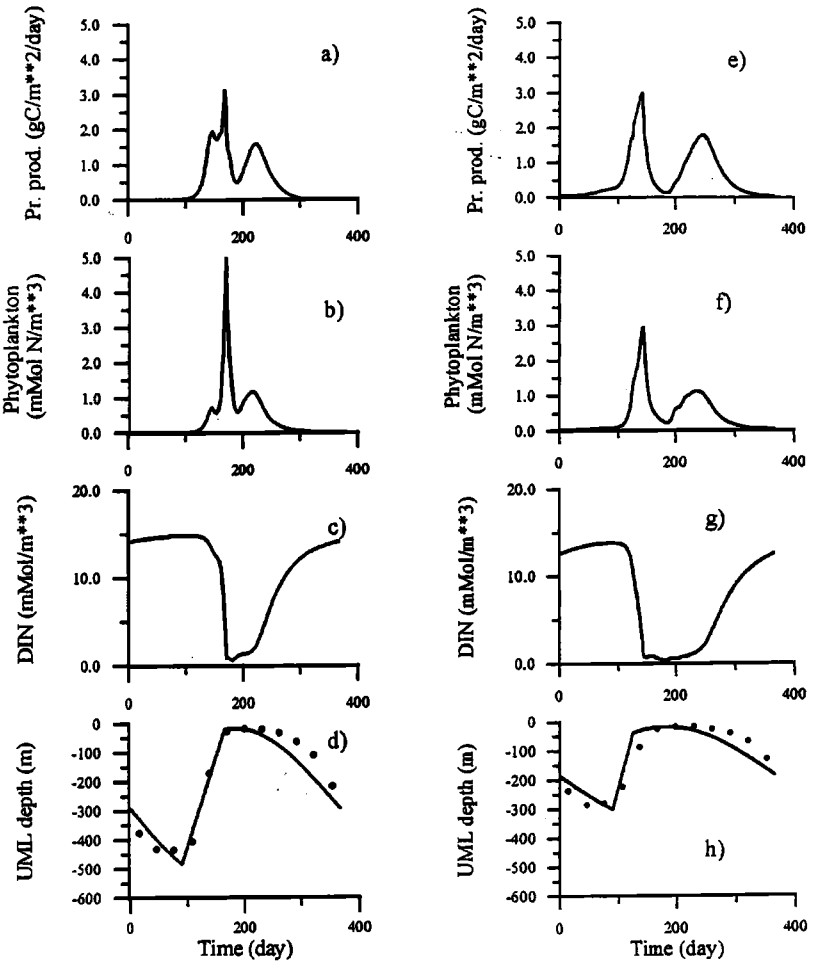

Figure 5. The simulated annual cycle of UML characteristics at (a-d) high latitudes and (e-h) midlatitudes of the Northern Hemisphere: Figures 5a and 5e show the primary production; Figures 5b and 5f show the phytoplankton biomass; Figures 5c and 5g show the DIN concentration; Figures 5d and 5h show the UML depth. The observed mean monthly UML depths (solid circles) were estimated using data from *Conkright et al.*, [1994] (see text); they were approximated by formula (A39) from the appendix (solid curves in Figures 5d and 5h).

limited spring production peak) characterizing four provinces located in the latitudinal zone between 40° and 60°N (one in the North Atlantic and three in the North Pacific). The features are (1) deep winter mixing with an entrainment of nutrient-rich water into the UML from the seasonal pycnocline; (2) light- and nutrient-limited primary production which is minimal during the summer and has a spring maximum constrained by nutrient availability; and (3) seasonal cycle of phytoplankton with a spring maximum and a second summer-autumn maximum which may occur at high latitudes. The only difference between our model and Longhurst's model is the second peak of primary production simulated in our model (Figures 5a and 5e) and absent in Longhurst. In support of our model, it is worth noting that observations of primary production in the UML at Ocean Weather Station I at 59°N, 19°W [*Parsons and Lalli*, 1988; *Williams*, 1988] show a pronounced peak in late August - early September. On the other hand, it is well known that a significant part of the total photic zone primary production during the summer period occurs below the UML in a deep chlorophyll maximum which is not reproduced by the model. This suggests that the model values of summer primary production might be underestimated, and it is not improbable that if the photic zone below UML was taken into account, then the second peak would not occur. It is also important that simulated mean annual primary production (0.49 and 0.63 gC m^{-2} d^{-1}, respectively, for high-latitude and midlatitude boxes of the Northern Hemisphere) is in good agreement with the estimate of 0.53 - 0.72 gC m^{-2} d^{-1} obtained by Longhurst for the provinces considered.

The low-latitude model boxes match those provinces which were generalized by Longhurst into model 3 (winter-spring production with nutrient limitation), appli-

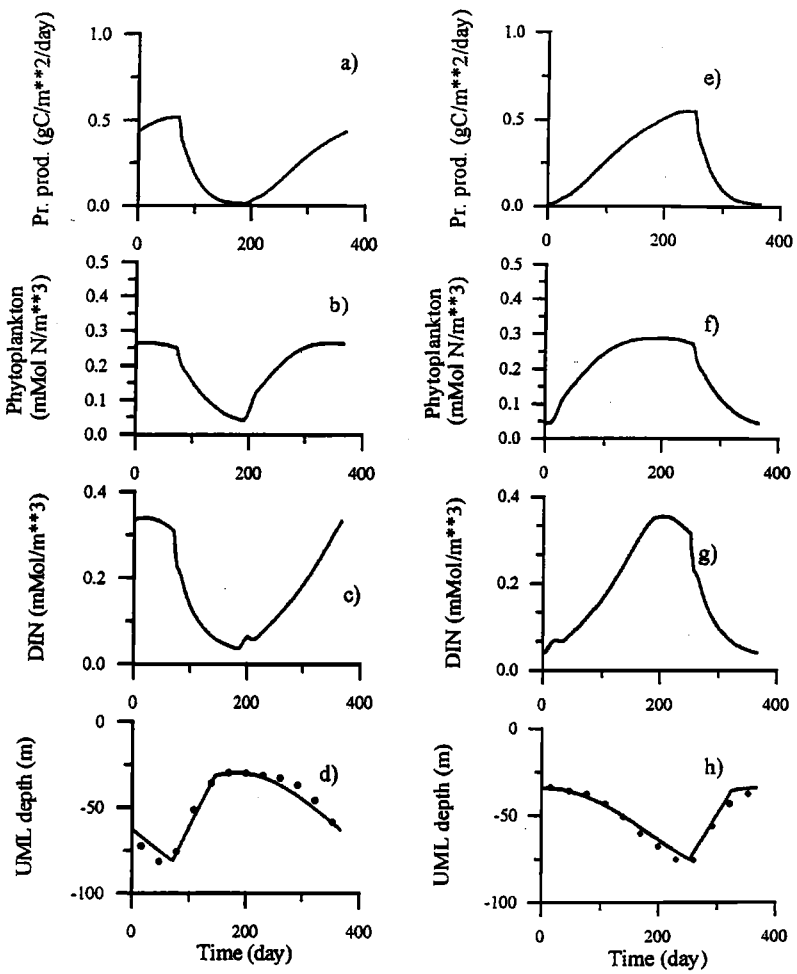

Figure 6. The same as Figure 5, except for the low latitudes of (a-d) Northern and (e-h) Southern Hemispheres.

cable to almost half the area of the world ocean, and model 4 (small-amplitude response to trade wind seasonality), relevant to about 20% of the whole ocean area where the seasonality of the UML depth is low. Simulated ecosystem dynamics in these boxes (Figure 6) has the specific features inherent in model 3: (1) the UML is relatively shallow; (2) primary production is not light limited and has a winter maximum due to the entrainment of nutrients; and (3) phytoplankton increases during the winter period and has a minimum in summer caused by the strong nutrient limitation. The higher values of DIN in the box below UML in the Southern Hemisphere (Figure 2) provide the higher mean annual primary production here (0.26 against 0.24 gC m^{-2} d^{-1} in the Northern Hemisphere). Both values are close to the lower limit of the range of mean annual production (from 0.19 to 0.59 $gC/m^2/d$) obtained by *Longhurst* [1995] for model 3.

In Longhurst's analysis the Southern Ocean was not exemplified by a specific model and provinces located within limits of it were attributed either to model 1 (polar irradiance-mediated production peak) or model 3. This makes comparison of our results with the Longhurst classification hard, and instead, we shall consider *Banse's* [1996] description of the seasonal phytoplankton production regime offshore in the Subantarctic water ring approximately coincident with the model surface midlatitude and high-latitude boxes in the Southern Hemisphere. According to *Banse* [1996] the regime has the following general features: (1) the chlorophyll concentration is low (of a few tenths of a mg/m^3) throughout the year in spite of the high nutrient concentration; (2) primary production is light limited during the austral winter and remains very low (about 0.1 gC m^{-2} d^{-1}) during the austral summer when it is not light limited; (3) chlorophyll concentration is independent of the UML depth during the austral winter and autumn. The simulated phytoplankton biomass (Figures 7b and 7f) does not exceed 0.3 mmol N/m^3 at the midlatitude box and 0.6 mmol N/m^3 at the high-latitude box, primary production (Figures 7a and 7e) is low during the whole year, DIN concentrations

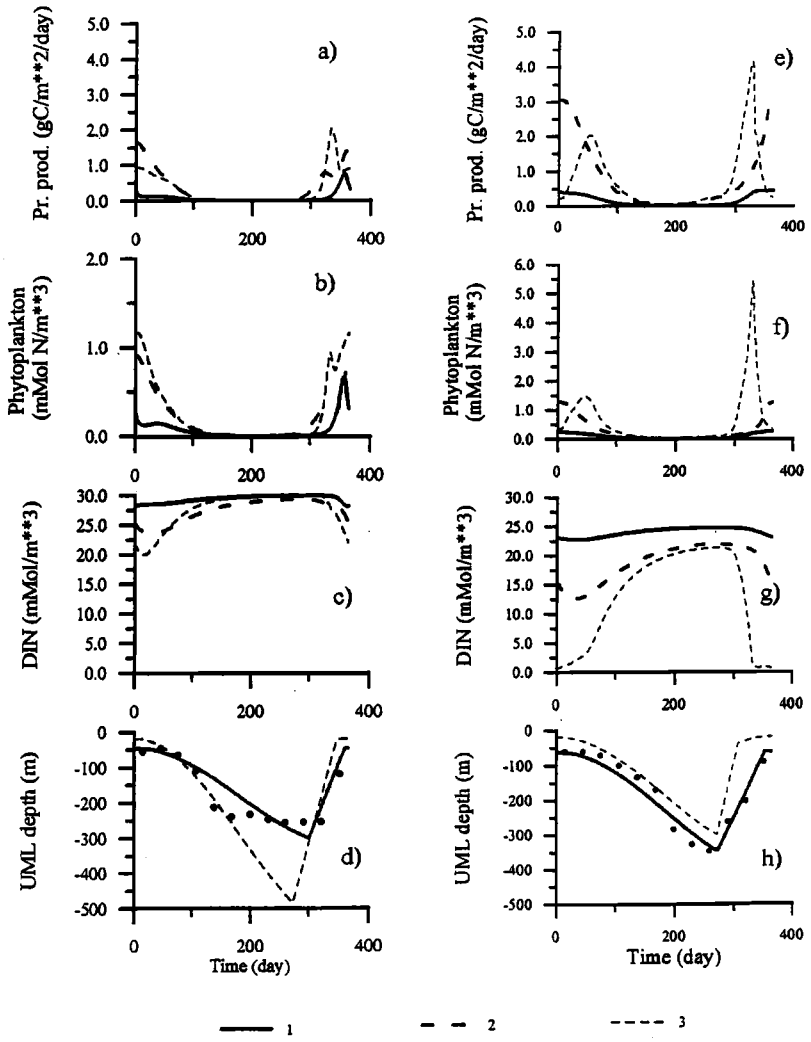

Figure 7. The same as Figure 5, except for the (a-d) high latitudes and (e-h) midlatitudes of the Southern Hemisphere. (Curves 1, 2, and 3 present the results of the control run, and experiments 2 and 3, respectively).

(Figures 7c and 7g) are nearly constant and very high (24 mmol N/m^3 and 29 mmol N/m^3 for the same boxes). Modeled mean annual primary production (0.15 and 0.07 gC m^{-2} d^{-1} at the midlatitudes and high latitudes, respectively) is in good agreement with values summarized by *Banse* [1996].

Bearing in mind the simplicity of the model structure and the rather arbitrary location of the boundaries between the simulated boxes, the simulated distributions of DIN, total inorganic carbon, and alkalinity are in a good agreement with the observations (Figures 2-4). Notice that these distributions in the Northern Hemisphere show a better fit to the data for the Atlantic Ocean than to those for the world ocean. This appears to be explained by the structure of the model which suggests the existence of a region of deep water formation in the Northern Hemisphere, whereas in reality this region exists only in the Atlantic Ocean and is absent in the Pacific.

4. Numerical Experiments

A set of numerical experiments was carried out in order to better understand the role of the Southern Ocean in the global carbon cycle and to estimate the range of natural variability of new production in this area. With this purpose, we started with the estimate of a potential new production for each model box, that is, a maximum new production that could be achieved by increasing the phytoplankton growth rate under the present-day external forcing (experiment 1). Further, assuming that in the case of iron abundance the ecosystem dynamics of the Southern Ocean becomes similar to that of the North Atlantic, the solution in

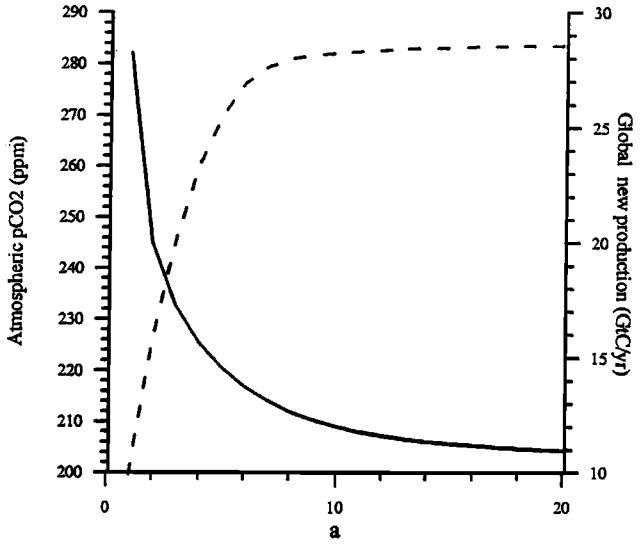

Figure 8. Dependencies of the atmospheric pCO_2 (solid curve) and global new production (dashed curve) on the coefficient a of increase in the phytoplankton growth rate and initial slope of the $P - I$ curve with respect to their standard values (see text).

the case of a globally uniform ecosystem model was obtained (experiment 2). It can be considered as a reasonable guide to the estimate of the possible increase of productivity due to the iron fertilization.

Before the iron hypothesis was proposed, it had been widely believed that low phytoplankton productivity in the Southern Ocean was connected with large UML depths during the summer which are substantially greater there than at the same latitudes in the North Atlantic [e.g. *Holm-Hansen et al.*, 1977]. To estimate the contribution of this effect to the formation of the HNLC conditions in the Southern Ocean, we obtained the model solution for the globally uniform ecosystem and UML depths in the Southern Ocean prescribed to be equal to those in the high-latitude and midlatitudes boxes of the Northern Hemisphere (experiment 3). Needless to say, there are other physical factors which may be responsible for the difference in phytoplankton productivity between a midlatitude and high-latitude zone of the South and North Atlantic (HNLC conditions against LNHC ones). The most important of them seem to be: (1) different ventilation of deep ocean by the OTHC in the Northern and Southern Hemispheres that provides the higher nutrient concentration in the latter region, and (2) lower temperature in the Southern Ocean that might reduce the phytoplankton growth rate. To estimate how changes in the vertical mixing variations in the Southern Ocean could influence oceanic new production and atmospheric pCO_2, the solution for different seasonal cycles of the UML depth in the Southern Ocean, which are determined by parameters $h_{\min}$ and $h_{\max}$ (see (A39) in the appendix), was obtained for the initial ecosystem model used in the control run (experiment 4). To estimate the combined effect of iron fertilization and possible UML depth changes in the Southern Ocean, we repeated experiment 4 for the globally uniform ecosystem (experiment 5).

As the initial condition for all numerical experiments, the preindustrial state of the ocean obtained in the control run was used.

4.1. Experiment 1: Potential New Production

The phytoplankton growth rate was increased by multiplying of α and V_p simultaneously by a factor a. The dependence of global new production and atmospheric pCO_2 on the factor a is given in Figure 8. As seen, both curves reach limiting values of about 29 Gt C/yr for the global new production and 204 ppm for the atmospheric pCO_2, respectively, at a=10 and a=20. Thus the maximum possible increase of new production is about 19 Gt C/yr. The spatial distribution of the maximum potential new production (Table 2) shows two salient features: (1) the production decreases in comparison with the control run results (a=1) at low latitudes and increases at midlatitudes and high latitudes, and (2) midlatitudes and high latitudes of the Southern Hemisphere contribute 78% (14.5 Gt C/yr) to the global new production increase.

The first feature is associated with the difference between ecosystem functioning at low and high latitudes (transport-dominated system against biology-dominated as defined by *Sarmiento et al.* [1993]). This difference indicates factors that are crucial for new production if the entrainment velocity is fixed. These are phytoplankton uptake rate limited by light and grazing for the biology-dominated systems and DIN concentration in the pycnocline for the transport-dominated systems.

In our case the decrease of new production at low latitudes can be explained in the following way. The increase of phytoplankton growth rate leads initially to an imbalance between the annual new and export production (the latter exceeds the former). This results in the vertical redistribution of DIN with higher deep and lower surface and intermediate layer concentrations when the equilibrium state is achieved. The lowered DIN concentration in the layer just below the UML causes a fall (about 1 Gt C/yr) in new production. Similarly, *Sarmiento and Orr* [1991] have obtained a reduction of new production in the equatorial region as a result of increasing the biological pump and complete nutrient removal in surface waters.

The large contribution of high latitudes and midlatitudes of the Southern Hemisphere to the global maximum potential new production is due to the higher

Table 2. Mean Annual New Production and Atmospheric pCO_2 for the Control Run and Experiments 1, 2, and 3

	New Production							pCO_2
	Northern Hemisphere			Southern Hemisphere			Global	of
	High Latitudes	Mid-latitudes	Low Latitudes	Low Latitudes	Mid-latitudes	High Latitudes	Value	Atmosphere
Control run	0.5	2.0	3.3	3.5	0.5	0.1	9.9	282
Experiment 1	2.1	5.6	3.0	2.7	10.8	4.3	28.6	204
Experiment 2	0.5	2.0	3.3	3.5	2.0	0.3	11.6	270
Experiment 3	0.5	2.0	3.3	3.5	2.6	0.3	12.3	262

(than in the Northern Hemisphere) DIN content, which in turn is connected with the features of the OTHC (see preceding section). In comparison with the present-day values, new production might be increased by 25 times in the Southern Ocean, and by only 3 times at the same latitudes of the Northern Hemisphere. Interestingly, the maximum potential new production at the midlatitudes of the Southern Hemisphere (8% of the total ocean area) is about 11 Gt C/yr, which approximately equals the model present-day global new production.

It should be noticed that our estimate of the maximum potential new production turned out to be less than it would be if the DIN concentration below the UML had remained unchanged (such an estimate has been obtained, for example, by *Martin* [1990]). In fact, in our model the increase in the phytoplankton growth rate caused a decrease of this concentration everywhere except for high latitudes of the Southern Hemisphere (cf. Figures 2a and 9a), which, of course, reduced somewhat the maximum potential new production.

It is of importance to note that the maximum value of potential new production is reached when the mean annual UML DIN concentrations differ significantly from zero (Figure 9a). The limiting concentrations of DIN which cannot be utilized by phytoplankton are determined by the DIN concentration below the UML and, to an even greater extent, by the duration of the winter when the phytoplankton utilization of nutrients is extremely low. As the duration is maximal at high latitudes, the maximal limiting concentrations of unutilized DIN occur there, contributing 1.8 and 4.9 mmol N/m^3, respectively, in the Northern and Southern Hemisphere.

In order to demonstrate the importance of taking account of seasonality in the model, we estimated the global potential new production assuming that surface nutrients might be completely depleted. In this case the mean annual new production is equal to the product of the DIN concentration below the UML and the sum of the entrainment and vertical velocities. The ocean potential new production turned out to be 37.9 Gt C/yr for the world ocean and 18.2 Gt C/yr for the Southern Ocean (against 28.6 Gt C/yr and 15.1 Gt C/yr in the case of the seasonal model).

To our knowledge, there are two earlier model estimates of a possible increase of the global new production as a result of complete nutrient utilization in the euphotic layer of the Southern Ocean [*Joos et al.*, 1991a,b; *Sarmiento and Orr*, 1991]. According to a 3-D model study of *Sarmiento and Orr* [1991], the complete nutrient depletion in the Southern Ocean, which was taken to be located south of 31°S occupying 18% of the total ocean area, leads to an increase in new production of 12-14 Gt C/yr. Using the high-latitude advection-diffusion (HILDA) model, *Joos et al.* [1991a,b] found

a) Experiment 1 (The potential new production)

	60-70N	40-60N	0-40N	0-40S	40-60S	60-70S
UML	1.8	0.3	0.04	0.04	0.4	4.9
z_{UML}-450m	9.2	10.0	5.8	6.6	19.1	33.4
450-1000m	9.2	10.0	24.5	23.0	19.1	33.4
1000-4000m	9.2	22.7		32.2		33.4

b) Experiment 2 (Uniform ecosystem)

	60-70N	40-60N	0-40N	0-40S	40-60S	60-70S
UML	10.7	7.9	0.17	0.18	18.7	27.4
z_{UML}-450m	15.9	16.4	6.6	8.4	24.6	30.6
450-1000m	15.9	16.4	27.4	29.1	24.6	30.6
1000-4000m	15.9	21.6		30.4		30.6

c) Experiment 3 (Uniform ecosystem and the same UML in both hemispheres)

	60-70N	40-60N	0-40N	0-40S	40-60S	60-70S
UML	10.7	7.9	0.17	0.19	13.1	27.6
z_{UML}-450m	15.9	16.4	6.6	7.1	24.3	30.8
450-1000m	15.9	16.4	27.4	29.0	24.3	30.8
1000-4000m	15.9	21.6		30.6		30.8

Figure 9. The DIN concentration (mmol/m^3) in the model boxes as calculated (a) in experiment 1, (b) in experiment 2, and (c) in experiment 3.

that the same effect on the 16% of the total ocean area contributes only 5.5 Gt C/yr. These two estimates are based on the assumption that surface nutrients can be completely utilized by phytoplankton, and in this regard they give an upperlimit value of the new production increase. Our estimate of 14.5 Gt C/yr of the new production increase turned out to be higher than either of the above two estimates despite the fact that in our model, there is no complete depletion of the surface nutrients and the area of the Southern Ocean is equal only to 10% of the total ocean area. The reason for the discrepancy between these estimates is a challenging question because of many distinctions between the three models (different ocean circulation and ecosystem submodels, different approximation of the world ocean and spatial resolution, the allowance for the seasonal changes in our model and the neglect of them in the models of *Joos et al.* [1991a,b] and *Sarmiento and Orr* [1991]. The differences in circulation models providing a greatly different nutrient supply to the surface layer of the Southern Ocean appear to be mainly responsible for this discrepancy. However, only an additional intercomparison study of these models could resolve this problem.

4.2. Experiment 2: Ocean With a Uniform Ecosystem

The equilibrium solution in this experiment is characterized by an increase of 1.7 Gt C/yr in the mean annual global new production and a decrease of 12 ppm in the mean annual atmospheric CO_2 as compared with the control run (Table 2). The mean annual DIN concentration is significantly changed only in the Southern Ocean (cf. Figures 2a and 9b): Its decrease in the UML at the midlatitudes and high latitudes amounts, respectively, to 4.9 and 1.7 mmol N/m^3. This additional utilization of DIN by phytoplankton results in an increase in the new production up to 2.0 and 0.3 Gt C/yr, or 19% and 7% of the maximum potential new production in the corresponding UML box (Table 2). According to the results of the preceding experiment (Figure 9a), 0.4 and 4.9 mmol N/m^3 of DIN, respectively, in the UML at the midlatitudes and high latitudes of the Southern Hemisphere are inaccessible for the utilization at all, and, hence, 18.3 and 22.5 mmol N/m^3 of DIN remain unutilized by phytoplankton. Thus light limitation and zooplankton grazing interfere long before the available DIN can be assimilated. As to seasonal changes in the ecosystem behavior, doubling of the phytoplankton growth rate in the Southern Ocean leads to an appreciable increase of primary production and phytoplankton biomass in the UML in the austral summer (Figure 7), although they still remain smaller than at the same latitudes of the Northern Hemisphere (cf. Figures 7 and 5).

The relatively weak sensitivity of the model solution to the doubling of the Southern Ocean growth rate implies that iron limitation of phytoplankton growth does not play a dominant role in the formation of the HNLC conditions in this region, and it is unlikely that any proposed iron fertilization of the Southern Ocean would have a pronounced effect on phytoplankton productivity and atmospheric pCO_2.

4.3. Experiment 3: Ocean With Uniform Ecosystem and the Same Seasonal Changes of the UML in Both Hemispheres

In this experiment the ecosystem characteristics as compared with experiment 2 are strongly changed only at the midlatitudes of the Southern Hemisphere (see Table 2, Figures 7 and 9). Here, as at the midlatitudes of the Northern Hemisphere, two phytoplankton blooms (rather than one as occurred in all preceding experiments) occur during the year. Thus if the annual cycle of the UML depth in the Southern Ocean were identical to that at the same latitudes of the Northern Hemisphere but just phase shifted by half a period, seasonal changes of the ecosystem characteristics at midlatitudes of the Southern and Northern Hemispheres would be not only qualitatively but also quantitatively rather similar (cf. Figures 5e-5g and 7e-7g). This is not the case for high-latitude regions (see Figures 5a-5d and 7a-7d). Despite higher DIN concentrations in the UML of the Southern Hemisphere throughout the year, the summer primary production and phytoplankton biomass in the high-latitude Southern Ocean turned out to be much less than in the Northern Hemisphere in this period. The reason is that the temperature in the latter region exceeds that in the former by $3^o - 4^o$C, raising the phytoplankton growth rate by 20-30%.

Despite the rather strong changes of ecosystem behavior at the midlatitudes of the Southern Hemispheres there was little effect on globally averaged characteristics: The global new production increases by 0.7 GtC/yr, and the atmospheric pCO_2 decreases by 8 ppm (see Table 2).

The results of experiments 2 and 3 imply that HNLC conditions in the midlatitude Southern Ocean are produced by the combined effect of the deep UML depth during the austral summer, iron limitation of phytoplankton productivity, and high nutrient concentration in the seasonal pycnocline. Within the high latitudes of the Southern Hemisphere, changes in the ecosystem characteristics due to iron limitation and minimal UML depths are comparatively small (Figures 7a-7c). Hence upwelling of nutrient-enriched deep water and perhaps low temperature hindering phytoplankton growth seem mainly to be responsible for the formation of the HNLC conditions.

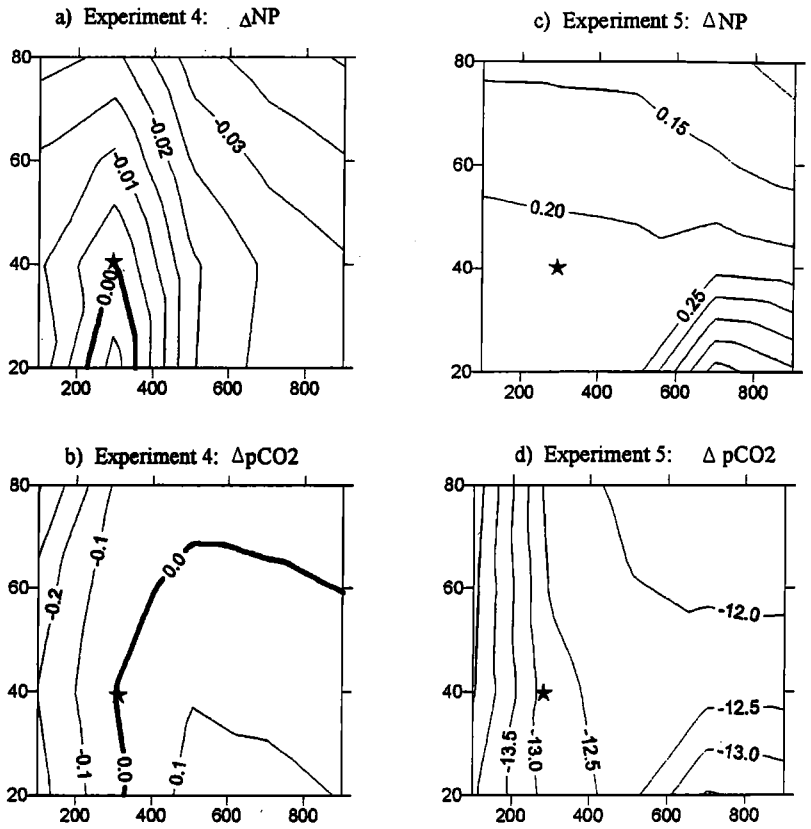

Figure 10. (a) Deviation of the new production (Gt C/yr) at midlatitudes of the Southern Hemisphere from values obtained in the control run as a function of parameters h_{max} and h_{min} in experiment 4. (b) Deviation of atmospheric pCO_2 from values obtained in the control run as a function of parameters h_{max} and h_{min} in experiment 4. (c) Same as Figure 10 a, except for experiment 5. (d) Same as Figure 10 b, except for experiment 5. Stars correspond to the values of h_{max} and h_{min} used in the control run.

4.4. Experiment 4: Sensitivity to Changes in UML Depth

The sensitivity of the model solution to variations in the UML depth at the midlatitudes of the Southern Hemisphere are illustrated in Figures 10a and 10b. Within the feasible range of h_{min} and h_{max} (from 20 to 80 m and from 100 to 900 m, respectively), changes of new production do not exceed 0.15 Gt C/yr (Figure 10a), that is 30% of its value in the control run. Such a relatively low sensitivity of the new production to changes in UML depth derives from the fact that the ecosystem in this region is a biology-dominated one for which, as discussed earlier, the phytoplankton growth rate is principally limited by light and zooplankton grazing.

Two major mechanisms are responsible for changes of atmospheric pCO_2 for the biology-dominated ecosystem in the case of UML depth variations. The first of these is the UML depth changes per se, which lead to changes in the UML-integrated new production and thus changes of the biological drawdown of TIC and atmospheric pCO_2. The second is connected with changes in the entrainment velocity and hence the supply of the TIC to the UML. These two mechanisms can, at least partly, compensate each other and therefore the relation between changes of the integrated new production and atmospheric pCO_2 is rather complicated. In particular, if changes of the UML depth lead to decrease of new production, atmospheric pCO_2 does not necessarily increase (as seen in Figures 10a and 10b, this occurs in the case of increasing h_{min} from its control run value ($\sim$ 60 m) at $h_{max} < 300$ m).

Because of the small changes in the new production in the region considered, the major role in the formation of surface TIC concentrations and atmospheric pCO_2 belongs to the entrainment velocity w_e. As seen (Figure 10b), changes of atmospheric pCO_2 are enhanced with decreasing the difference $\Delta h = h_{max} - h_{min}$ which determines the mean annual entrainment velocity $w_e = \Delta h/T$, where T is the annual period. A maximal decrease of about 16 ppm occurs in the upper left corner of the diagram at $h_{min} = 80$ m and $h_{max} = 100$ m.

Similar runs with changes in the UML depth were carried out for the high latitudes of the Southern Ocean. The results show maximal changes of about 0.04 Gt C/yr (40%) for the annual new production in this region and maximal changes of about 0.2 ppm in atmospheric pCO_2. The sensitivity of atmospheric pCO_2 to changes in the UML depth in this region turned out to be lower than for the midlatitude region. This is because of the lower vertical gradient of DIC (2 mmol/m^3 for high latitudes against 14 mmol/m^3 for midlatitudes) and lower area (2% of the total ocean are for high latitudes against 8% for midlatitudes).

4.5. Experiment 5: Combined Effect of the Changes in UML Depth and Biology

To estimate the consequences of the changes in UML depth in the Southern Ocean in the case of increased phytoplankton growth rate resulting from iron fertilization, experiment 4 was repeated assuming that ecosystem dynamics were the same everywhere. Effects of the changes in UML depth at the increased phytoplankton productivity are enhanced (cf. Figures 10a-10b and Figures 10c-10d).

Experiment 2 shows that iron fertilization of the Southern Ocean provides a 15 ppm drop in atmospheric pCO_2. Nevertheless *Peng and Broecker* [1991a,b] emphasized that the rate of vertical mixing is the key to evaluating the impact of any possible intensification of photosynthesis in this area. In the modeling study of *Mitchell et al.* [1991], it was concluded that without a mechanism for shallowing of the UML, Fe addition would fail to significantly mitigate atmospheric pCO_2. As seen from Figure 10d, if iron fertilization is accompanied by a shallowing of winter mixing to 150 m at the midlatitudes, this might double the effect of fertilization. As our experiments showed, similar changes of mixing at the high latitudes might add only 1 ppm.

Our results imply that changes in the mixing regime are able to provide an intensification of the effect of iron fertilization on reducing atmospheric pCO_2. Nevertheless this effect itself is so insignificant that it seems unlikely to be the principal mechanism for the observed variability of the atmospheric pCO_2 even under the conditions of increased stratification.

5. Implications for the Regulation of Atmospheric pCO_2

The results obtained in experiments 4 and 5 present an equilibrium response of the global carbon cycle in the ocean-atmosphere system to changes in phytoplankton growth rate and UML depth. They cannot be directly applied to estimate the effect of iron fertilization of the Southern Ocean on the continuing increase in atmospheric CO_2 content generated by the burning of fossil fuels and deforestation. However, they are applicable to the problem of understanding the low atmospheric pCO_2 level during the Last Glacial Maximum when the state of the ocean-atmosphere carbon system was likely to be in quasi-equilibrium. Two primary mechanisms that could reduce atmospheric pCO_2 during glacial periods have been suggested as operating in the Southern Ocean: increased biological productivity or lower vertical mixing [*Sarmiento and Toggweiler*, 1984; *Siegenthaler and Wenk*, 1984; *Knox and McElroy*, 1984]. *Martin* [1990] postulated that iron fertilization stimulated the efficiency of the biological pump throughout the glacial Southern Ocean. New records of complementary radionuclide proxies in sediments of the Atlantic and Indian sectors of the Southern Ocean indicated that Martin's hypothesis is valid only in the Subantarctic zone where export production increased dramatically, whereas in Antarctic waters to the south of the modern polar front (MPF), it was lower than during the interglacial period [*Kumar et al.*, 1995]. Nevertheless, *Kumar et al.* [1995] have demonstrated that the former effect prevails over the latter and the increase in export production can partly explain the lowering of CO_2 concentrations in the glacial atmosphere.

There is another group of paleogeochemical evidence supporting the idea about decreased vertical mixing in the glacial Southern Ocean (which is usually attributed to the effect of increased stratification in the upper ocean). *Morely and Hays* [1983] assumed that the abundance of the radiolarian *Cycladophora davisiana* in Antarctic sediments during the last glacial period indicates that the vertical hydrographic structure of the glacial Southern Ocean was similar to that of the modern Sea of Okhotsk, the only place in the world ocean where *Cycladophora davisiana* is abundant in modern sediments. This structure (a well-developed near-freezing layer underlying a highly seasonal surface layer) would have limited winter mixing to a depth of 100-200 m. More detailed information about changes in the Southern Ocean upper layer stratification during the last glacial period have been obtained by *Francois et al.* [1997], who estimated the supply rate of nitrate to surface waters by combining the export flux of nitrogen estimated from a suite of paleoproductivity proxies with information about the fraction of surface nitrate utilized by phytoplankton (evaluated using bulk sediment $\delta^{15}N$). Glacial surface water stratification was found to be increased south of the MPF and decreased north of it where export production was increased. The combined effect of these changes in stratification (and associated changes in vertical mixing) seems to have resulted in an overall increase in the mean surface nitrogen and carbon utilization and to have contributed to the lowering of glacial atmospheric pCO_2. According to preliminary

calculations performed with a modified CYCLOP S box model, this effect could account for ~ 50% of the glacial lowering in atmospheric pCO_2 [*Francois et al.*, 1997].

As our calculations showed, changes in vertical mixing (i.e., in h_{min} and h_{max} in our model) alone, even occurring throughout the whole Southern Ocean, could lead to no more than a 15 ppm decrease in the atmospheric pCO_2 (Figure 10b). On the other hand, atmospheric pCO_2 additionally decreases by 15 ppm in the absence of iron limitation in the Southern Ocean (Table 2, experiment 2). If these changes in Southern Ocean phytoplankton growth rate are accompanied by decreased vertical mixing (as a result, for example, of a decrease in the maximum UML depth h_{max} in our model) at the midlatitudes of the Southern Hemisphere, the total effect will be about 35 ppm (Figure 10d). As our experiments showed, a similar decrease in vertical mixing for the non-iron-limited high latitudes of the Southern Hemisphere could add no more than 1 ppm to this estimate.

Thus, contrary to the opinion of *Francois et al.* [1997], changes in vertical mixing in the Southern Ocean alone could hardly account for a significant part of the glacial lowering in atmospheric pCO_2. The same conclusion applies to the effect of iron fertilization of the Southern Ocean. However, the combined effect of these two factors could account for almost 50% of the pCO_2 lowering. Our estimates support the idea of *Peng and Broecker* [1991a,b] who emphasized that the vertical exchange of water in the Southern Ocean is the major factor limiting uptake of CO_2 by the ocean in response to iron fertilization.

6. Summary and Conclusions

The following conclusions can be drawn from the numerical experiments.

1. The model estimate of the global ocean new production outside of shelf regions is 9.9 Gt C/yr. The potential new production (new production which might be reached by an unlimited increase of phytoplankton growth rate) under present-day external forcing is 29 Gt C/yr and corresponds to an atmospheric pCO_2 of 205 ppm. A total of 76% of the global new production increase is contributed by the midlatitudes and high latitudes of the Southern Hemisphere (40°-70°S). Thus the carbon pump could theoretically be responsible for the observed low level of atmospheric pCO_2 during the last glaciation. However, this estimate is based on an unrealistic (tenfold) increase in the phytoplankton maximum growth rate and initial slope of the $P-I$ curve. This casts doubt on whether any realistic limits on the variability of phytoplankton productivity could be enough to provide changes of the pCO_2 level in the atmosphere comparable to the glacial-interglacial changes.

2. Iron limitation in the Southern Ocean plays a part in reducing the primary production, but it is not the only factor of importance. The HNLC conditions are also due to the high DIN concentrations below the UML and deep mixing during the austral summer. The maximum impact of iron fertilization alone on the lowering of atmospheric pCO_2 is about 10 ppm, and this implies that the low pCO_2 level of the last ice age might not be connected with the iron limitation.

3. Sensitivity of the atmospheric pCO_2 to changes in the UML depths in the Southern Ocean is insignificant. The maximum drop in atmospheric pCO_2 might be achieved by a shallowing of the UML during the austral winter and a deepening during the austral summer compared to present-day conditions. If these changes occur over the whole area of the Southern Ocean, the effect would not exceed 15 ppm. This low sensitivity implies that decreased mixing usually attributed to stronger stratification in the Southern Ocean during the last glacial period could not make a significant contribution to lowering the atmospheric pCO_2. These results also suggest that an indirect effect of the greenhouse warming on marine biota via changes in the high-latitude mixing regime cannot significantly affect the level of pCO_2 in the atmosphere.

4. Changes in vertical mixing in the Southern Ocean are able to double the effect of iron fertilization on the lowering of atmospheric pCO_2. The combined effect might amount to about 30-35 ppm for the whole area of the Southern Ocean, which could account for not more than one half of the glacial lowering of about 80 ppm.

5. An increase of export production due to changes in vertical mixing is not necessarily accompanied by a lowering of the atmospheric pCO_2. Hence without information about changes in the UML depth, one should be careful on drawing conclusions about changes in atmospheric pCO_2 from paleogeochemical evidence of export production changes.

Appendix: Model Equations

Equations of the budget of state variables in the model boxes (Figure 1) are written as

$$\frac{d}{dt}X_{jsi}V_{si} - s_iX_{jsi}w_{ei} = \delta_{5j}Q_i^a s_i - Q^X_{hi-0\ ji}s_i + \\ +\delta_{3j}Gr_{si}(D) + \delta_{6j}Gr_{si}(H) + V_{si}B_{jsi} + Adv_{jsi}, \quad \text{(A1)}$$

$$\frac{d}{dt}X_{jti}V_{ti} + s_iX_{jti}w_{ei} = Q^X_{hi+0\ ji}s_i + \\ \delta_{3j}Gr_{ti}(D) + \delta_{6j}Gr_{ti}(H) + V_{ti}B_{jti} + Adv_{jti}, \quad \text{(A2)}$$

$$\frac{d}{dt}X_{jdi}V_{di} = \delta_{3j}Gr_{di}(D) + \delta_{6j}Gr_{di}(H) + \\ +V_{di}B_{jdi} + Adv_{jdi},\ i = \pm1, \pm2, \pm3;\ \ j = 1, ..., 7 \quad \text{(A3)}$$

$$\frac{d}{dt}C_a = \sum_i s_i Q_i^a, \tag{A4}$$

where advective transport terms for the Northern Hemisphere appear as

$$Adv_{js1} = q_1 \frac{h_{s2}}{h_{b2}}(X_{js2} - X_{js1}), \tag{A5}$$

$$Adv_{jt1} = q_1\left(\frac{h_{s2}}{h_{b2}}X_{js1} + \frac{h_{b2} - h_{s2}}{h_{b2}}X_{jt2} - X_{jt1}\right), \tag{A6}$$

$$Adv_{jd1} = q_1(X_{jt1} - X_{jd1}) + q_e(X_{jd2} - X_{jd1}), \tag{A7}$$

$$Adv_{js2} = q_1\frac{h_{s2}}{h_{b2}}(X_{jt2} - X_{js2}) + \\ + q_2\frac{h_{s3}}{h_{b3}}(X_{js3} - X_{js2}), \tag{A8}$$

$$Adv_{jt2} = q_1\left(\frac{s_2}{s_2 + s_3}X_{jd1} + \frac{s_3}{s_2 + s_3}X_{jd2} - \right. \\ \left. - X_{jt2}\right) + q_2\left(\frac{h_{s3}}{h_{b3}}X_{js2} + \frac{h_{b3} - h_{s3}}{h_{b3}}X_{jt3} - X_{jt2}\right), \tag{A9}$$

$$Adv_{jd2} = q_1\frac{s_3}{s_2 + s_3}(X_{jd1} - X_{jd2}) + \\ + q_2(X_{jt2} - X_{jd2}) + q_e\left(\frac{h_{b2} - h_{b3}}{h_{b2}}X_{jd-2} + \right. \\ \left. + \frac{h_{b2} - h_{b3}}{h_{b2}}X_{jt3} - X_{jd2}\right), \tag{A10}$$

$$Adv_{js3} = q_2\frac{h_{s3}}{h_{b3}}(X_{jt3} - X_{js3}), \tag{A11}$$

$$Adv_{jt3} = q_2(X_{jd2} - X_{jt3}) + q_e\frac{h_{b3}}{h_{b2}}(X_{jt-3} - X_{jt3}). \tag{A12}$$

Advective transport terms for the Southern Hemisphere might be written in a similar manner according to the advection scheme shown in Figure 1.

The turbulent fluxes $Q^X_{hi-0\ ji}$ and $Q^X_{hi+0\ ji}$ at the lower boundary of the UML are parameterized as

$$\begin{aligned} Q^X_{hi-0\ ji} &= (X_{jsi} - X_{jti})w_{ei} \quad w_{ei} > 0, \\ Q^X_{hi-0\ ji} &= 0 \quad w_{ei} \le 0, \end{aligned} \tag{A13}$$

$$\begin{aligned} Q^X_{hi+0\ ji} &= 0 \quad w_{ei} \le 0, \\ Q^X_{hi+0\ ji} &= -(X_{jsi} - X_{jti})w_{ei} \quad w_{ei} > 0. \end{aligned} \tag{A14}$$

Inner biological sources and sinks in the UML are written in the form (index i is omitted)

$$B_{1s} = Pr - G_1 - De_1, \tag{A15}$$

$$B_{2s} = \beta_1 G_1 + \beta_2 G_2 - De_2, \tag{A16}$$

$$B_{3s} = (1 - \beta_1)G_1 - \beta_2 G_2 - De_3 + De_1 + \delta De_2, \tag{A17}$$

$$B_{4s} = -Pr + \varepsilon De_2 + De_3, \tag{A18}$$

$$B_{5s} = R_{C/N}B_{4s} - R_{Ca/N}Pr + Ds_s, \tag{A19}$$

$$B_{6s} = R_{Ca/N}(B_{3s} + De_3) - Ds_s, \tag{A20}$$

$$B_{7s} = B_{4s} - 2B_{1s}R_{Ca/N} - 2B_{6s}. \tag{A21}$$

Following *Fasham et al.* [1993] and *Ryabchenko et al.* [1997], functions Pr, De_1, De_2, De_3, G_1, and G_2 are given as

$$Pr = JQP, \tag{A22}$$

$$J = \frac{2}{h}\int_0^{t^0}\int_0^h F(I_0(\tau)\exp\{-(k_w + k_c P)z\})dzd\tau, \tag{A23}$$

$$F(I) = \frac{V_p \alpha I}{(V_p^2 + \alpha^2 I^2)^{1/2}}, \quad V_p = V_p^* a^T, \tag{A24}$$

$$Q = \frac{N}{k_1 + N}, \tag{A25}$$

$$De_1 = \frac{\mu_1 P^2}{k_5 + P}, \quad De_2 = \frac{\mu_2 Z^2}{k_6 + Z}, \quad De_3 = \mu_3 D, \tag{A26}$$

$$G_1 = \frac{gp_1 P^2 Z}{k_3(p_1 P + p_2 D) + p_1 P^2 + p_2 D^2}, \\ G_2 = \frac{gp_2 D^2 Z}{k_3(p_1 P + p_2 D) + p_1 P^2 + p_2 D^2}. \tag{A27}$$

The parameterization of degradation of the detritus hard parts $Ds_{s,t,d\ i}$ is taken from *Heinze et al.* [1991] where justification and parameter values can be found.

Inner biological sources and sinks below the UML are expressed as

$$B_{3t,d} = -\lambda D_{t,d}, \tag{A28}$$

$$B_{4t,d} = \lambda D_{t,d}, \tag{A29}$$

$$B_{5t,d} = R_{C/N}B_{4t,d} + Ds_{t,d}, \tag{A30}$$

$$B_{6t,d} = -Ds_{t,d}, \tag{A31}$$

$$B_{7t,d} = -B_{4t,d} + 2Ds_{t,d}. \tag{A32}$$

The particle flux through the water column is parameterized as

$$Gr_{si}(Y) = -(s_i w_g Y_{si})\Psi, \tag{A33}$$

$$Gr_{t\pm1}(Y) = (s_{\pm1}w_g(Y_{s\pm1} - Y_{t\pm1}) + \\ + \omega De_{2\pm1}\frac{V_{s\pm1}}{V_{t\pm1}})\Psi, \tag{A34}$$

$$Gr_{t\pm2}(Y) = (s_{\pm2}w_g(Y_{s\pm2} - Y_{t\pm2}) + \\ \omega De_{2\pm2}\frac{V_{s\pm2}}{V_{t\pm2}})\Psi, \tag{A35}$$

$$Gr_{t\pm3}(Y) = (s_{\pm3} w_g Y_{s\pm3} + \omega De_{2\pm3} \frac{V_{s\pm3}}{V_{t\pm3}})\Psi, \quad \text{(A36)}$$

$$Gr_{d\pm2}(Y) = (s_{\pm1} w_g (Y_{t\pm1} - Y_{d\pm2}))\Psi, \quad \text{(A37)}$$

$$Gr_{d\pm3}(Y) = (w_g (s_{\pm2} Y_{t\pm2} + s_{\pm1} Y_{d\pm2}))\Psi, \quad \text{(A38)}$$

where Ψ=1 for $Y = D$ and $\Psi = R_{Ca/N}$ for $Y = H$. Expressions (A37) and (A38) imply that there is no precipitation of detritus on the ocean bottom.

The annual cycle of the UML depth is calculated using the formula

$$\begin{aligned} h(t) &= -(h_{\max} - h_{\min})(\sin\frac{\pi(\mathrm{t}+\mathrm{T})}{\mathrm{T}} - 1)/ \\ &\quad (\sin\frac{\pi \mathrm{t}_1}{\mathrm{T}} + 1) + \mathrm{h}_{\min} \quad 0 \le \mathrm{t} \le \mathrm{t}_1, \\ h(t) &= h_{\min} + (t - t_1)(h(t_2) - h(t_1))/(t_2 - t_1) \\ &\quad t_1 < t < t_2, \\ h(t) &= -(h_{\max} - h_{\min})(\sin\frac{\pi \mathrm{t}}{\mathrm{T}} - 1)/ \\ &\quad (\sin\frac{\pi \mathrm{t}_1}{\mathrm{T}} + 1) + \mathrm{h}_{\min} \quad \mathrm{t}_2 \le \mathrm{t} \le \mathrm{T}, \quad \text{(A39)} \end{aligned}$$

where $T = 365$ days is the annual period and t_1 and t_2 are the times of the beginning and end of a jump in the UML depth. According to (A39), the seasonal changes of h in each UML model box (Figures 5-7) are uniquely determined by values of $h_{\max}$, $h_{\min}$, t_1, and t_2.

Notation

- A total alkalinity.
- Adv advective transport.
- α initial slope of $P - I$ curve, equal to 0.1 $(\mathrm{Wm}^{-2})^{-1}\mathrm{d}^{-1}$.
- B_{jsi}, B_{jti}, B_{jdi} functions describing the total effect of inner biological sources and sinks of variable j.
- β_1, β_2 assimilation coefficients of zooplankton, equal to 0.75, 0.75.
- C concentration of the total inorganic carbon.
- C_a content of the CO_2 in the atmosphere.
- D concentration of the organic part of detritus.
- $(\,)_d$ index indicating the deep boxes.
- dt model time step.
- Ds degradation rate of the detritus hard parts.
- De_1 rate of phytoplankton natural mortality.
- De_2 rate of zooplankton losses due to excretion, natural mortality, and grazing of higher-order predators.
- De_3 rate of breakdown of detritus to DIN.
- δ_{kj} Kronecker symbol.
- δ fraction of the total zooplankton losses transformed into detritus, equal to 0.3.
- ε fraction of the total zooplankton losses transformed into DIN, equal to 0.6.
- G_1, G_2 grazing rates of the zooplankton on the phytoplankton and detritus.
- $Gr_{si}(Y)$, $Gr_{ti}(Y)$, $Gr_{di}(Y)$ functions describing particle flux through the water column; $Y = (D, H)$.
- g zooplankton maximum growth rate, equal to 1 d^{-1}.
- H concentration of the inorganic part of detritus.
- h_{si} UML depth at the outcrop regions.
- h_{bi} depth of the lower boundaries of the water masses.
- $I_0(\tau)$ photosynthetically active radiation (PAR) immediately below the surface of the water (assumed to be proportional to the absorbed total solar radiation at the sea surface with the coefficient λ_p (0.41)).
- $()_i$, $i = \pm1, \pm2, \pm3$ indexes indicating the surface, intermediate, and deep water masses, respectively, in the Northern (plus sign) and Southern (minus sign) Hemispheres.
- J light-limited growth rate.
- $()_j$, $j = 1, ..., 7$ number of the state variable.
- k_1 half-saturation constant for DIN uptake, equal to 0.5 $\mathrm{mmol/m}^3$.
- k_3 grazing parameter, equal to 1 $\mathrm{mmol/m}^3$).
- k_5 half-saturation constant for phytoplankton mortality, equal to 0.2 $\mathrm{mmol/m}^3$.
- k_6 half-saturation constant for zooplankton loss rate, equal to 0.2 $\mathrm{mmol/m}^3$.
- k_w light attenuation due to water, equal to 0.04 m^{-1}.
- k_c phytoplankton self-shading coefficient equal to 0.03 $\mathrm{m}^2\ \mathrm{mmol}^{-1}$.
- λ detritus breakdown rate below the UML, equal to 0.05 d^{-1}.
- μ_1 phytoplankton mortality rate, equal to 0.05 d^{-1}.
- μ_2 zooplankton mortality rate, equal to 0.25 d^{-1}.
- μ_3 detritus breakdown rate in the UML, equal to 0.05 d^{-1}.
- N concentration of the DIN.
- ω part of zooplankton losses transforming into fast sinking detritus, which is considered to be instantly exported from the UML into the underlying layer, equal to $1 - \varepsilon - \delta$).
- P phytoplankton biomass.
- Pr daily average primary production.
- p_1 relative grazing preference for phytoplankton, equal to 0.6.
- p_2 relative grazing preference for detritus, equal to 0.4.
- Q non-dimensional DIN limiting factor.
- Q_i^a flux of CO_2 at the ocean-atmosphere boundary.

$Q^X_{hi-0\ ji}$, $Q^X_{hi+0\ ji}$ turbulent fluxes of variable j at the lower UML boundary and the upper boundary of the underlying box in water mass i.

$q_{\pm 1}$ volume transport between surface and intermediate water masses.

$q_{\pm 2}$ volume transport between the intermediate and deep water masses.

q_e cross-equatorial volume transport.

$R_{C/N}$ Redfield ratio, equal to 6.6.

$R_{Ca/N}$ ratio of calcium to nitrogen in phytoplankton, equal to 0.07.

S salinity.

$(\ )_s$ index indicating the UML.

s_i areas of outcrop region of water mass i.

T temperature.

t time.

τ fraction of the day, equal to 0 at sunrise and t^0 at noon.

$(\ )_t$ index indicating the intermediate boxes just below the UML.

V_{si}, V_{ti}, V_{di} volumes of the boxes.

V_p^* maximum growth rate of phytoplankton.

w_e entrainment velocity at lower boundary of the UML, equal to dh_s/dt.

w_g detritus sinking velocity, equal to 4m d^{-1}.

$\{X_{jsi}\}$ vector of state variables in the UML of water mass i, equal to $\{P_{si}, Z_{si}, D_{si}, N_{si}, C_{si}, H_{si}, A_{si}\}$.

$\{X_{jti}\}$ vector of state variables in the intermediate boxes of water mass i, equal to $\{0, 0, D_{ti}, N_{ti}, C_{ti}, H_{ti}, A_{ti}\}$.

$\{X_{jdi}\}$ vector of state variables in the deep boxes of the intermediate and deep water masses, equal to $\{0, 0, D_{di}, N_{di}, C_{di}, H_{di}, A_{di}\}$.

Z zooplankton biomass.

Acknowledgments. This research was supported by INTAS grant 96-1917. We are grateful to T.R. Anderson for many useful discussions.

References

Antoine, D., J.-M. Andre, and A. Morel, Oceanic primary production, 2, Estimation at global scale from satellite (coastal zone color scanner) chlorophyll, *Global Biogeochem. Cycles 10*, 57-69, 1996.

Bainbridge, A., *Hydrographyc Data, 1972-1973, GEOSECS Atlanic Expedition*, vol. 1, U.S. Gov. Print. Off., Washington, D.C., 1981.

Banse, K., Rates of phytoplankton cell division in the field and in iron enrichment experiment, *Limnol. Oceanogr., 36*, 1886-1898, 1991.

Banse, K., Low seasonality of low concentration of surface chlorophyll in the Subantarctic water ring: Underwater irradiance, iron or grazing?, *Prog. Oceanogr., 37*, 241-291, 1996.

Berger, W.H., K. Fiscer, C. Lai, and G. Wu, Oceanic primary productivity and organic carbon flux, 1, Overview and maps of primary production and export, *Rep. 87-30*, pp.1-67, Scripps Inst. of Oceanogr., La Jolla, Calif. 1987.

Bolin, B., A. Bjorkstrom, K. Holmen, and B. Moore, The simultaneous use of tracers for ocean circulation studies, *Tellus, 35B*, 206-236, 1983.

Broecker, W.S., Ocean chemistry during glacial time, *Geochim. Cosmochim. Acta, 46*, 1689-1705, 1982.

Broecker, W.S., and T.-H. Peng, *Tracers in the Sea*, 690 pp., Lamont-Doherty Earth Observatory, Palisades, N.Y., 1982.

Broecker, W.S., and T.-H. Peng, Glacial to Interglacial changes in the operation of the global carbon cycle, *Radiocarbon, 28*, 309-327, 1986.

Broecker, W.S., D. Spencer, and H. Craig. *Hydrographyc Data, 1973-1974, GEOSECS Pacific Expedition*, vol. 3, U.S. Gov. Print. Off., Washington, D.C., 1982.

Conkright, M.E., S. Levitus, and T.P. Boyer, *World Ocean Atlas 1994*, vol.1, *Nutrients*, Natl. Oceanic and Atmos. Admin., Washington, D.C., 1994.

Ducklow, H.W., Ocean biogeochemical fluxes: New production and export of organic matter from the upper ocean, *U.S. Nat. Rep. Int. Union Geod. Geophys. 1991-1994, Rev. Geophys., 33*, 1271-1276, 1995.

Epply, R.W., and B.J. Peterson, Particulate organic matter flux and planktonic new production in the deep ocean, *Nature, 282*, 677-680, 1979.

Fasham, M.J.R., Variations in the seasonal cycle of biological production in subarctic oceans: A model sensitivity analysis, *Deep Sea Res., 42*, 1111-1149, 1995.

Fasham, M.J.R., J.L. Sarmiento, R.D. Slater, H.W. Ducklow, and R. Williams, Ecosystem behaviour at Bermuda station "S" and Ocean Weather Station India: A general circulation model and observational analysis, *Global Biogeochem. Cycles, 7*, 379-415, 1993.

Francois, R., M.A. Altabet, E.-F. Yu, D.M. Sigman, M.P. Bacon, M. Frank, G. Bohrmann, G. Bareille and L.D. Labeyie, Contribution of the Southern Ocean surface-water stratification to low atmospheric CO_2 concentrations during the last glacial period, *Nature, 389*, 929-935, 1997.

Frost, B.W., A modelling study of processes regulating plankton standing stock and production in the open subarctic Pacific, *Prog. in Oceanogr., 32*, 17-57, 1993.

Girdjuk, G.V., B.N. Egorov, and S.P. Malevskii-Malevich, *Determination of Radiance Balance at the Ocean Surface*, 148 pp, Gydrometeoizdat, St. Petersburg, 1992.

Han, Y.-J., and S.-W. Lee, A new analysis of monthly mean wind stress over the global ocean. *Rep. 26.*, Clim. Res. Inst. and Dep. of Atmos. Sci., Oregon State Univ. 150 pp., 1981.

Heinze, C., E. Maier-Reimer, and K.Winn, Glacial pCO_2 reduction by the world ocean: Experiments with the Hamburg carbon cycle model, *Paleoceanography, 6*, 395-430, 1991.

Holm-Hanzen, O., S.Z. El-Sayed, G.A. Franceschini, and R.L. Cunel, Primary production and the factors controlling phytoplankton growth in the Southern Ocean, in *Adaptations Within Antarctic Ecosystems*, edited by G. A. Llano, Smithsonian Institution, pp. 11-50, 1977.

Houghton, J.T., L.G. Meria Filho, J. Bruce, H. Lee, B.A. Callander, E. Haites, N. Harris, and K. Maskell, *Climate Change 1994: Radiative Forcing of Climate Change and an Evaluation of the IPCC IS92 Emission Scenarios*, Cambridge Univ. Press, New York, 1995.

Joos, F., J.L. Sarmiento, and U. Siegenthaler, Estimates of the effect of Southern Ocean iron fertilization on atmospheric CO_2 concentrations, *Nature, 349*, 772-775, 1991a.

Joos, F., U. Siegenthaler, and J.L. Sarmiento, Possible effect of iron fertilization in the Southern Ocean on atmospheric CO_2 concentration, *Global Biogeochem. Cycles*, *5*, 135-150, 1991b.

Kagan, B.A., and N.B. Maslova, Non-uniqueness of the thermohaline circulation in a three-layer ventilated ocean, *Fluid Dyn. Res.*, *8*, 287-295, 1991.

Keir, R.S., On the late Pleistocene ocean geochemistry and circulation, *Paleoceanography*, *3*, 413-445, 1988.

Knox, F., and M.B. McElroy, Changes in atmospheric CO_2: Influence of the marine biota at high latitude, *J. Geophys. Res.*, *89*, 4629-4637, 1984.

Kumar, N., R.F. Anderson, R.A. Mortlock, P.N. Froelich, P. Kubik, B. Dittrich-Hannen, and M. Suter, Increased biological productivity and export production in the glacial Southern Ocean, *Nature*, *378*, 675-680, 1995.

Lampitt, R.S., and A.N. Antia, Particle flux in deep seas: Regional characteristics and temporal variability, *Deep Sea Res.*, *44*, 1377-1403, 1996.

Levitus, S., Climatological Atlas of the World Ocean, *NOAA Prof. Pap. 13*, U.S. Gov. Print. Off., Washington, 1982.

Levitus, S., R. Burgett, and T.P. Boyer, *World Ocean Atlas 1994, vol. 3, Salinity*, U.S. Department of Commerce, NOAA, Washington, D.C., 1994.

Levitus, S., and T.P.Boyer, *World Ocean Atlas 1994, Vol.4: temperature*, Natl. Oceanic and Atmos. Admin., Washington, D.C., 1994.

Lochte, K., H.W. Ducklow, M.J.R. Fasham, and C. Stienen, Plankton succession and carbon cycling at 47°N 20°W during the JGOFS North Atlantic Bloom Experiment, *Deep Sea Res. II*, *40*, 91-114, 1993.

Longhurst, A., Seasonal cycles of pelagic production and consumption, *Prog.Oceanogr.*, *36*, 77-167, 1995.

Longhurst, A., S. Sathyendranath, T. Platt, C. Caverhill, An estimate of global primary production in the ocean from satellite radiometer data, *J. Plankton Res.*, *17*, 1245-1271, 1995.

Martin, J.H., Glacial-interglacial change: The iron hypothesis, *Paleoceanography*, *5*, 1-13, 1990.

Martin J.H., G.A. Knauer, D.M. Karl, and W.W. Broenkow, VERTEX: Carbon cycling in the northeast Pacific, *Deep Sea Res.*, *34*, 267-285, 1987.

Martin, J.H., S.E. Fitzwater and R.M. Gordon, Iron deficiency limits phytoplankton growth in Antarctic waters, *Global Biogeochem. Cycles*, *4*, 5-12, 1990.

Mitchell, B.J., E.A. Brody, O. Holm-Hansen, C. McClain, and J. Bishop, Light limitation of phytoplankton biomass and macronutrient utilization in the Southern Ocean, *Limnol. Oceanogr.*, *36*, 1662-1677, 1991.

Morely, J.J., and J.D. Hays, Oceanographic conditions associated with high abundances of the radiolarian *Cycladodophora davisiana*, *Earth Planet. Sci. Lett.*, *66*, 63-72, 1983.

Najjar R.G., J.L. Sarmiento, and J.R.Toggweiler, Downwards transport and fate of organic matter in the ocean: Simulations with a general circulation model, *Global Biogeochem. Cycles*, *6*, 45-76, 1992.

Palmer, J.R., and I. Totterdell, Production and export in a global ocean ecosystem model, *Deep Sea Res.*, in press, 1999.

Parsons, T.R., and C.M. Lalli, Comparative oceanic ecology of the plankton communities of the subarctic Atlantic and Pacific Oceans. *Oceanogr. and Mar. Biol. Annu. Rev.*, *26*, 317-359, 1988.

Peng, T.-H., and W.S. Broecker, Dynamical limitations on the Antarctic iron fertilization strategy, *Nature*, *349*, 227-229, 1991a.

Peng, T.-H., and W.S. Broecker, Factors limiting the reduction of atmospheric CO_2 by iron fertilization, *Limnol. Oceanogr.*, *36*, 1919-1927, 1991b.

Ryabchenko, V.A., M.J.R. Fasham, B.A. Kagan, and E.E. Popova, What causes short-term oscillations in ecosystem models of the ocean mixed layer?, *J. Mar. Syst.*, *13*, 33-50, 1997.

Ryabchenko, V.A., V.A. Gorchakov and M.J.R. Fasham, Seasonal dynamics and biological productivity in the Arabian Sea euphotic zone as similated by a three-dimensional ecosystem model, *Global Biogeochem. Cycles*, *12*, 501-530, 1998.

Sarmiento, J.L., Slowing the buildup of fossil CO_2 in the atmosphere by iron fertilization: A comment. *Global Biogeochem. Cycles*, *5*, 1-2, 1991.

Sarmiento, J.L., and J.C. Orr, Three-dimensional simulations of the impact of Southern Ocean nutrient depletion on atmospheric CO_2 and ocean chemistry, *Limnol. and Oceanogr.*, *36*, 1928-1950, 1991.

Sarmiento, J.L., and J.R. Toggweiler, A new model for the role of the oceans in determining atmospheric pCO_2, *Nature*, *308*, 621-624, 1984.

Sarmiento, J.L., R.D. Slater, M.J.R. Fasham, H.W. Ducklow, J.R. Toggweiler and G.T. Evans, A seasonal three-dimensional ecosystem model of nitrogen cycling in the North Atlantic euphotic zone, *Global Biogeochem. Cycles*, *7*, 417-450, 1993.

Sarmiento, J.L., T.M.C. Hughes, R.J. Stouffer, and S. Manabe, Ocean carbon cycle response to future greenhouse warming, *Nature*, *393*, 245-249, 1998.

Siegenthaler, U., and J.L. Sarmiento, Atmospheric carbon dioxide and the ocean. *Nature*, *365*, 119-125, 1993.

Siegenthaler, U., and T. Wenk, Rapid atmospheric CO_2 variations and oceanic circulation. *Nature*, *308*, 624-626, 1984.

Six, K.D., and E. Maier-Reimer, Effects of plankton dynamics on seasonal carbon fluxes in an ocean general circulation model, *Global Biogeochem. Cycles*, *10*, 559-583, 1996.

Sundquist, E.T., Geological perspectives on carbon dioxide and the carbon cycle, in *The Carbon Cycle and Atmospheric CO_2: Natural Variations Archean to Present, Geophys. Monogr. Ser.*, vol. 32, edited by E.T. Sundquist and W.S. Broecker, pp. 5-59, AGU, Washington, D.C., 1985.

Takahashi, T., R.A. Feely, R.F. Weiss, R.H. Wanninkhof, D.W. Chipman, S.C. Sutherland and T.T. Takahashi, Global air-sea flux of CO_2: An estimate based on measurements of sea-air pCO_2 difference, *Proc. Natl. Acad. Sci. U.S.A.*, *94*, 8292-8299, 1997.

Toggweiler, J.R., and J.L. Sarmiento, Glacial to interglacial changes in atmospheric carbon dioxide: The critical role of ocean surface water in high latitudes, in *The Carbon Cycle and Atmospheric CO_2: Natural Variations Archean to Present, Geophys. Monogr. Ser.*, vol. 32, edited by E.T. Sundquist and W.S. Broecker, pp. 163-184, AGU, Washington, D.C., 1985.

Weaver, A.J., and T.M.C. Hughes, Stability and variability of the thermohaline circulation and its link to climate, *Trends Phys. Oceanogr. Ser.*, 56 pp., Counc. of Sci. Res. Integration, 1992.

Wenk, T., and U. Siegenthaler, The high-latitude ocean as a control of atmospheric CO_2, in *The Carbon Cycle and Atmospheric CO_2: Natural Variations Archean to Present, Geophys. Monogr. Ser.*, vol. 32, edited by E.T. Sundquist and W.S. Broecker, pp. 185-194, AGU, Washington, D.C., 1985.

Williams R., Spacial heterogeneity and niche differentiation in oceanic zooplankton, *Hydrobiologia, 167/168*, 151-159, 1988.

M.Fasham and E.Popova, Southampton Oceanography Centre, Empress Dock, Southampton SO14 3ZH, England. (e-mail: mike.fasham@soc.soton.ac.uk; ekaterina.popova@soc.soton.ac.uk)

V.Ryabchenko, St. Petersburg Branch, P.P. Shirshov Institute of Oceanology, Russian Academy of Sciences, 30, Pervaya Liniya, 199053 St. Petersburg, Russia. (e-mail: rya@gk3103.spb.edu)

(Received October 27, 1998; revised April 14, 1999; accepted April 28, 1999.)